Metadata of the chapter that will be visualized online

Chapter Title	Developments in the Photonic Theory of Fluorescence	
Copyright Year	2016	
Copyright Holder	Springer International Publishing Switzerland	
Author	Family Name	**Leeder**
	Particle	
	Given Name	**Jamie M.**
	Suffix	
	Division	School of Chemistry
	Organization	University of East Anglia
	Address	Norwich NR4 7TJ, UK
Author	Family Name	**Bradshaw**
	Particle	
	Given Name	**David S.**
	Suffix	
	Division	School of Chemistry
	Organization	University of East Anglia
	Address	Norwich NR4 7TJ, UK
Author	Family Name	**Williams**
	Particle	
	Given Name	**Mathew D.**
	Suffix	
	Division	School of Chemistry
	Organization	University of East Anglia
	Address	Norwich NR4 7TJ, UK
Corresponding Author	Family Name	**Andrews**
	Particle	
	Given Name	**David L.**
	Suffix	
	Division	School of Chemistry
	Organization	University of East Anglia
	Address	Norwich NR4 7TJ, UK
	Email	d.l.andrews@uea.ac.uk

Abstract

Conventional fluorescence commonly arises when excited molecules relax to their ground electronic state, and most of the surplus energy dissipates in the form of photon emission. The consolidation and full development of theory based on this concept has paved the way for the discovery of several mechanistic variants that can come into play with the involvement of laser input – most notably the phenomenon of multiphoton-induced fluorescence.

However, other effects can become apparent when off-resonant laser input is applied during the lifetime of the initial excited state. Examples include a recently identified scheme for laser-controlled fluorescence. Other systems of interest are those in which fluorescence is emitted from a set of two or more coupled nanoemitters. This chapter develops a quantum theoretical outlook to identify and describe these processes, leading to a discussion of potential applications ranging from all-optical switching to the generation of optical vortices.

Keywords (separated by '-') Multiphoton process - Anisotropy - Nonlinear optics - Optical vortex - All-optical switch

Chapter 10
Developments in the Photonic Theory of Fluorescence

Jamie M. Leeder, David S. Bradshaw, Mathew D. Williams, and David L. Andrews

Abstract Conventional fluorescence commonly arises when excited molecules relax to their ground electronic state, and most of the surplus energy dissipates in the form of photon emission. The consolidation and full development of theory based on this concept has paved the way for the discovery of several mechanistic variants that can come into play with the involvement of laser input – most notably the phenomenon of multiphoton-induced fluorescence. However, other effects can become apparent when off-resonant laser input is applied during the lifetime of the initial excited state. Examples include a recently identified scheme for laser-controlled fluorescence. Other systems of interest are those in which fluorescence is emitted from a set of two or more coupled nanoemitters. This chapter develops a quantum theoretical outlook to identify and describe these processes, leading to a discussion of potential applications ranging from all-optical switching to the generation of optical vortices.

Keywords Multiphoton process • Anisotropy • Nonlinear optics • Optical vortex • All-optical switch

10.1 Introduction

Fluorescence is a form of luminescence whose measurement is widely employed in optical devices, microscopy imaging, biology and medical research. The basic theory describing fluorescence emission from individual molecules is extremely well-established. It centres upon the release of a photon from an excited molecule as it relaxes in a transition that is spin-allowed, and usually electric dipole-allowed, to a lower electronic state; this follows an initial electronic excitation, and usually some intervening vibrational relaxation. Delving more deeply into this model, the underlying quantum theory offers us additional physical insights into single- and multi-photon fluorescence. It also enables the prediction of several other novel, fluorescence-related processes, potentially leading to the production of useful

J.M. Leeder • D.S. Bradshaw • M.D. Williams • D.L. Andrews (✉)
School of Chemistry, University of East Anglia, Norwich NR4 7TJ, UK
e-mail: d.l.andrews@uea.ac.uk

C.D. Geddes (ed.), *Reviews in Fluorescence 2015*,
DOI 10.1007/978-3-319-24609-3_10

devices and applications across the sciences. This chapter offers a look at the latest developments in the photonic theory of fluorescence.

The structure of this work is as follows. Section 10.2 first affords a brief outline of the fundamental formalism utilized throughout this chapter, working up from quantum amplitudes to expressions for measurable rates of fluorescence, cast in terms that can duly elicit photonic attributes of the processes they describe. This section provides a basis for understanding the connection and common ground between the most familiar form of fluorescence, and the newer processes. It also includes a summary of the way in which the theory can be developed as a two-state model, whenever optical response is dominated by just the excited and ground electronic levels. Successive sections address recent research on specific applications. Section 10.3 discusses advances in the theory of multiphoton fluorescence, casting expressions for the output signals in terms of the associated electric polarization and molecular transition moment properties. Results established by means of an isotropic orientational average determine the fluorescence response of a fully disordered molecular environment – a complete system, or micro-domains within a complete system – also revealing one means by which multiphoton imaging can be further developed to monitor and quantify variations in chromophore orientation. Section 10.4 explores the development of 'laser-controlled fluorescence', a process whereby the rate of fluorescent emission is modified by an off-resonant probe beam of sufficient intensity. Associated changes in fluorescence behaviour afford new, chemically-specific information and a potential for novel technological applications through all-optical switching. Finally, in Sect. 10.5, theoretical developments in the field of multi-emitter fluorescence are described. Following a focus on the quantum mechanisms that operate between a pair of electromagnetically coupled nanoantenna emitters, attention is then given to designer systems based on an arrangement of molecular nanoemitters – which can be used as a basis for the generation of optical vortex radiation. Simple illustrations of the topics to be discussed in Sects. 10.3, 10.4 and 10.5 are shown in Fig. 10.1 The chapter concludes in Sect. 10.6 with a Discussion.

10.2 Photonic Theory of Fluorescence

In any molecular system that exhibits fluorescence, the primary stage – associated with the absorption of input radiation – is the electronic excitation of individual chromophores. Typically, ultrafast intramolecular vibrational redistribution produces a degree of immediate relaxation that results in a partial degradation of the acquired energy, with subsequent fluorescence occurring from the lowest level of the electronic excited state. For present purposes, assuming the validity of a Born-Oppenheimer separation of wavefunctions, we can focus on the character of these electronic transitions, since it is these that primarily determine the energetics and selection rules. The corresponding vibrational energies are generally small compared to the difference in electronic energy states: their impact on the fluorescence

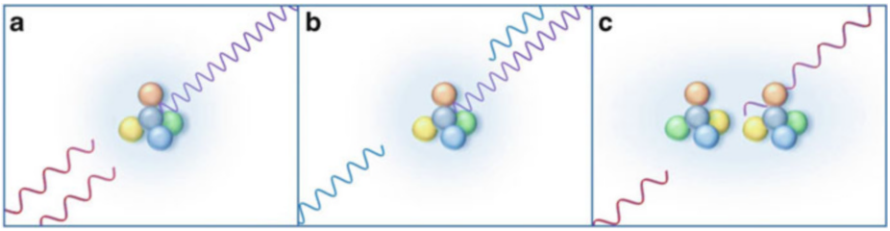

Fig. 10.1 Variations on molecular fluorescence: (**a**) Multiphoton fluorescence; (**b**) Laser-controlled fluorescence; (**c**) Fluorescence from coupled nanoemitters

transition, although important, principally features in the linewidth, determined by Franck-Condon factors.

With these considerations, the following representation of theory can now be built on the basis of parameters delivered by a quantum framework for both the radiation and the matter. Specifically, these will essentially be the quantum amplitudes (strictly 'matrix elements', M_{FI}, as they are in principle derivable for any specified pair of states) for the initial excitation and for the fluorescent decay, duly representing the input and output photons as quanta of the radiation field. Assuming that the energy associated with the strength of coupling between matter and radiation is far less than any molecular bond energy, such matrix elements which characterize the transition between initial and final system states, $|I\rangle$ and $|F\rangle$ respectively, are typically derived through time-ordered perturbation theory [1]. Such a perturbation is formally cast as an infinite, converging series, *i.e.*:

$$M_{FI}(\xi) = \sum_{n=1}^{\infty} \langle F|H_{\text{int}}(\xi)(T_0 H_{\text{int}}(\xi))^{n-1}|I\rangle, \tag{10.1}$$

where ξ represents a molecule or chromophore label, $T_0 = (E_I - H_0)^{-1}$ (in which E_I is the energy of the initial state and H_0 is the Hamiltonian for an unperturbed system), and $H_{\text{int}}(\xi)$ is the interaction Hamiltonian whose operation defines the system perturbation. The development of Eq. (10.1) usually involves implementation of the completeness relation $\sum_R |R\rangle\langle R| = 1$ etc., so that the expression becomes;

$$\begin{aligned} M_{FI} = &\langle F|H_{\text{int}}|I\rangle + \sum_R \frac{\langle F|H_{\text{int}}|R\rangle\langle R|H_{\text{int}}|I\rangle}{(E_I - E_R)} + \sum_{R,S} \frac{\langle F|H_{\text{int}}|S\rangle\langle S|H_{\text{int}}|R\rangle\langle R|H_{\text{int}}|I\rangle}{(E_I - E_R)(E_I - E_S)} \\ &+ \sum_{R,S,T} \frac{\langle F|H_{\text{int}}|T\rangle\langle T|H_{\text{int}}|S\rangle\langle S|H_{\text{int}}|R\rangle\langle R|H_{\text{int}}|I\rangle}{(E_I - E_R)(E_I - E_S)(E_I - E_T)} + \ldots \quad , \end{aligned} \tag{10.2}$$

where the intermediate system states are given by $|R\rangle$, $|S\rangle$, $|T\rangle\ldots$ and E_N is the energy of the state denoted by its subscript; the leading non-zero term for a process

involving n photons is generally the nth term. The interaction Hamiltonian is explicitly expressed in the following form, featuring $\mu_i(\xi)$ as a component of the electric dipole operator:

$$H_{\text{int}}(\xi) = -\varepsilon_0^{-1}\mu_i(\xi) \cdot d_i^{\perp}(\mathbf{R}_\xi), \tag{10.3}$$

using the convention of summation over repeated Cartesian subscripts. Here, the contributions of magnetic and higher-order transition moments are legitimately ignored; the contribution from both are typically insignificant under conditions in which the molecular dimensions are significantly smaller than the optical wavelength. The transverse electric displacement field operator $d_i^{\perp}(\mathbf{R}_\xi)$ at position $\mathbf{R}_\xi$ acts upon the radiation system states within the arbitrary quantization volume V as:

$$d_i^{\perp}(\mathbf{R}_\xi) = \sum_{\mathbf{p},\eta} \left(\frac{\hbar c p \varepsilon_0}{2V}\right)^{\frac{1}{2}} i\left[e_i^{(\eta)}(\mathbf{p})a^{(\eta)}(\mathbf{p})\exp(i\,\mathbf{p}.\mathbf{R}_\xi) - \overline{e}_i^{(\eta)}(\mathbf{p})a^{\dagger(\eta)}(\mathbf{p})\exp(-i\,\mathbf{p}.\mathbf{R}_\xi)\right], \tag{10.4}$$

where $e_i^{(\eta)}$ is the unit electric polarization vector, with an overbar denoting its complex conjugate. The electric field operator is linear in both a and $a^\dagger$, which are the optical mode annihilation and creation operators, respectively, for a mode ($\mathbf{p}$, η); hence each operation of $d_i^{\perp}(\mathbf{R}_\xi)$ is responsible for either the creation or annihilation of a single photon. The parameter n in Eq. (10.1) defines the order of the matrix element with respect to $H_{\text{int}}(\xi)$, therefore effectively being determined by the number of matter-radiation interactions that occur within a given optical process. In order to exact results amenable to practical verification, it is common practice to report results in a form based on a measurable experimental observable. Throughout this review a commonly deployed methodology is utilized through application of Fermi's Golden Rule:

$$\Gamma = \frac{2\pi\rho_F}{\hbar}\left\langle |M_{FI}|^2 \right\rangle. \tag{10.5}$$

In this expression, Γ is the rate observable, proportional to the modulus square of the relevant matrix element, while on the right-hand side ρ_F represents a density of final system states defined as the number of molecular levels per unit energy associated with $|F\rangle$; the angular brackets here denote an orientational average to be effected for a system of randomly oriented molecules, as in the liquid phase [2]. Moreover, when the initial excitation is the rate-determining step (as is usually the case), then an effective rate can be cast in terms of an average for the product of matrix element quadratic terms for the excitation and fluorescent emission.

Equation (10.2) is often modified by the introduction of a simplifying assumption, to describe the optical response of a model system with just two electronic states (although, when applied to some other kinds of optical interaction, this common simplification can produce significantly misleading predictions) [3]. In

the context of fluorescence, it is in most cases entirely defensible to consider only the ground and lowest excited states, *i.e.* employ the two-state model [4–18], since Kasha's rule states that fluorescence only occurs in appreciable yield from the lowest electronic excited state – although it cannot be presumed that the state from which the fluorescence decay occurs is necessarily the same as the state initially populated by photoexcitation. Upon application of such a two-state strategy, the quantum completeness identity becomes;

$$1 = \sum_{R} |R\rangle\langle R| \equiv \sum_{\rho, r} |\rho_{\mathrm{rad}}\rangle |r_{\mathrm{mol}}\rangle\langle r_{\mathrm{mol}}|\langle\rho_{\mathrm{rad}}| = \mathbf{1}_{\mathrm{rad}} \times (|0\rangle\langle 0| + |\alpha\rangle\langle\alpha|). \qquad (10.6)$$

where the system state is decomposed into radiation and molecular states, the latter involving only a ground state $|0\rangle$ and a first excited state $|\alpha\rangle$. Limiting any intermediate molecular states to just $|0\rangle$ and $|\alpha\rangle$ restricts the number of transition sequences from the excited to ground molecular states. In complex interactions, each sequence generates a combined sequence of transition electric dipole moments, such as $\boldsymbol{\mu}^{0\alpha}$ and $\boldsymbol{\mu}^{\alpha 0}$, in combination with the static dipole moments of the ground and excited energy levels, $\boldsymbol{\mu}^{00}$ and $\boldsymbol{\mu}^{\alpha\alpha}$ respectively. It can be legitimately assumed that the former transition electric moments are real (as is always possible, given a suitable choice of basis set for the molecular wavefunctions) and therefore equal, by virtue of the Hermiticity of the dipole operator. Detailed analysis reveals that the dependence on static moments emerges only in terms of their vector difference. With the benefit of an algorithmic method, the following prescription, $\boldsymbol{\mu}^{\alpha\alpha} \rightarrow \boldsymbol{\mu}^{\alpha\alpha} - \boldsymbol{\mu}^{00} = \mathbf{d}$; $\boldsymbol{\mu}^{00} \rightarrow 0$ can be adopted [19], whose general validity has been proven to rest on a canonical transformation of the quantum interaction operator [20]. Applying this protocol requires application of an associated rule: any transitional mechanism that connects the initial and final system states (here, for the emission process) through a ground state static dipole is discarded.

10.3 Multiphoton Fluorescence

In laser-based studies of fluorescence, it is well-known that polarization features of the emission convey rich information on structural details of the sample, particularly in condensed phase molecular media. For example, detailed information can be secured on the degree of chromophore orientational order through polarization-resolved measurements [21, 22]. Numerous studies have focused on confined, highly ordered materials where the chromophores are held in crystalline structures [23–25], or else samples such as cell membranes, molecular films or fibers, where they are less rigidly bound to a physical matrix [26, 27]. In such instances, the rotational freedom of the targeted species is commonly restricted, enforcing a degree of orientational order relative to the external structure. Whereas polarization-derived information is often restricted to two spatial dimensions, the

determination of three-dimensional orientation can also be explored [28]. Further investigations have extended the scope of such studies into the single-molecule regime, to elucidate information that is obscured in ensemble studies [29–31].

This section assesses the output signal resulting from *multiphoton* induced fluorescence, the application of which is highly prevalent in modern research owing primarily to the technique's unparalleled ability to deliver high-resolution, three dimensional imaging of heterogeneous samples. In general terms, the capture of high quality images aids the investigation of chemically specific information, since fluorescence intensity distributions allow the determination of the relative location, concentration and structure of specific molecular species *in situ* [32–34]. However, the attendant advantages offered by multiphoton methods include further features that have as yet received surprisingly little attention. In this respect it shall be shown that multiphoton imaging has a potential for further development as a diagnostic tool, to selectively discriminate micro-domains within a sample that exhibit a degree of orientational correlation. Any such technique could then equally monitor dynamical changes in this localized order, perhaps resulting from a chemical interaction, or acting in response to an externally applied stimulus.

The theory that follows duly provides a means of interrogating the extent of correlation between the transition moments associated with the process of fluorescence, namely those responsible for photon absorption and emission. Specific attention is given to the extent to which fluorescence retains a directionality of polarization from the initial excitation. To approach such issues involved in multiphoton processes, it is appropriate to begin with a representation of the optical process in its entirety, subsuming both the multi-photon absorption of laser input and the emission of fluorescent radiation. The output optical signal, $I_{\mathrm{flu}}^{(n)}(\phi)$, is thus introduced as a function of the experimentally controllable angle between the polarization vector of the incident light and the resolved polarization of the emission, ϕ:

$$I_{\mathrm{flu}}^{(n)}(\phi) = K^{(n)} \sum_{\xi} \left\langle \left| M_{\nu 0}^{(n)}(\xi) \right|^2 |M_{0\alpha}(\xi)|^2 \right\rangle. \tag{10.7}$$

The signal separates matrix elements for nth order multiphoton absorption and single – photon emission, $M_{\nu 0}^{(n)}(\xi)$ and $M_{0\alpha}(\xi)$ respectively. The possibility for excited state processes such as internal conversion, hindered rotation, rotational diffusion, intramolecular energy transfer etc. are accommodated through the adoption of labels 0 and ν to denote the molecular ground and initially excited energy levels, and α for the level from which emission occurs. The fluorescence signal in Eq. (10.7) is thus portrayed in terms of the physically separable efficiencies of the absorption and emission processes; the constant of proportionality $K^{(n)}$ is itself dependent on experimental parameters including the nth power of the mean irradiance delivered by the input laser beam, and also the corresponding degree of nth order coherence [35]. Angular brackets once again denote implementation of an orientation average, providing for the likely case in which the transition moments

associated with multiphoton absorption and single photon emission are randomly oriented relative to the propagation vector of the input. If rotational diffusion during the excited state lifetime is significant, then the orientational average itself decouples into separate averages for the excitation and decay processes. To determine the results for one-, two- and three-photon induced fluorescence, the form of all associated matrix elements is required. Each is derived by standard methods; the underlying principles are introduced in a detailed description of single-photon induced fluorescence that directly follows.

10.3.1 One-Photon Induced Fluorescence

As indicated above, the theory for the process of single-photon induced fluorescence is characterized by the development of two distinct matter-radiation interactions: the first describes the optical excitation of a chromophore by single-photon absorption; the second entails molecular relaxation and photon emission that returns the chromophore to its ground electronic state. Addressing first the former process, the matrix element for single photon absorption is derived by substitution of Eq. (10.3) into (10.1) where $n = 1$:

$$M_{\nu 0}^{(1)}(\xi) = -i\left(\frac{q\hbar c p}{2\varepsilon_0 V}\right)^{\frac{1}{2}} e_i^{(\eta)} \mu_i^{\nu 0} \exp(i\,\mathbf{p}\cdot\mathbf{R}_\xi). \tag{10.8}$$

The level of intensity of the input mode is such it conveys q photons within a quantization volume V that is assumed to enclose the absorbing chromophore. By comparison, the matrix element for the process of photon emission, which engages electronic decay of the excited chromophore and the creation of a single photon into the vacuum radiation field, is expressed as:

$$M_{0\alpha}(\xi) = i\left(\frac{\hbar c\, p'}{2\varepsilon_0 V}\right)^{\frac{1}{2}} \overline{e}_i^{(\eta')} \mu_i^{0\alpha} \exp\left(-i\,\mathbf{p}'\cdot\mathbf{R}_\xi\right). \tag{10.9}$$

Here, prime labels have been utilized to distinguish the wave-vector and polarization of the output fluorescence from corresponding properties of the input beam. By substituting the matrix elements for both absorption and emission into Eq. (10.7), a complete expression for the signal output emerges:

$$I_{\text{flu}}^{(1)}(\phi) = \sum_{\xi} K^{(1)} \left\langle S_{ij}\overline{S}_{kl} T_{ij}\overline{T}_{kl} \right\rangle, \tag{10.10}$$

where the square modulus of Eqs. (10.8) and (10.9) have been employed, and the products of scalar parameters within the parentheses of each matrix element are incorporated into the proportionality constant $K^{(1)}$. For ease of notation, the

orientation-dependent products of the unit electric polarization vectors, and those of the molecular transition moments, are each incorporated into second rank tensors where specifically S_{ij} and $\overline{S}_{ij}$ denote $e_i^{(\eta)}\overline{e}_j^{(\eta')}$ and $\overline{e}_i^{(\eta)}e_j^{(\eta')}$. Likewise, the molecular transition moment products described by T_{ij} and $\overline{T}_{ij}$ correspond to $\mu_i^{\nu 0}\mu_j^{0\alpha}$ and $\overline{\mu}_i^{\nu 0}\overline{\mu}_j^{0\alpha}$. Here, and in all subsequent applications of this notation, the last index in the electric polarization and molecular transition tensors relates to the photon emission. Equation (10.10) thus expresses a result that embraces the angular disposition of the chromophore transition moments with respect to the input and output polarization vectors. In a rigidly oriented system, forgoing the orientational average, the result would thus exhibit a dependence on $\cos^2\eta\cos^2\theta$, where η is the angle between the absorption moment and the input polarization, and θ is that between the emission moment and the fluorescence polarization.

10.3.2 Multiphoton Induced Fluorescence

Having derived the matrix element for one-photon emission, the fluorescence signal for multiphoton processes now requires expressions that account for the concerted absorption of two or more photons. First addressing the specific case of *two-photon* absorption, the associated matrix element entails a progression through an intermediate system state in which one photon is annihilated and the chromophore, lacking a resonant level to match the photon energy, is accordingly in a transient superposition of virtual molecular states. Any such energy non-conserving state can be sustained only as long as is allowed by the time-energy uncertainty principle – necessary summation is made over all possible intermediate states, as required by quantum principles. The full matrix element is thus developed by substitution of Eqs. (10.3) and (10.4) into Eq. (10.1) where $n = 2$ such that:

$$M_{\nu 0}^{(2)}(\xi) = \left(\frac{q_2^{1/2}\hbar c p}{2\varepsilon_0 V}\right) e_i^{(\eta)} e_j^{(\eta)} \alpha_{(ij)}^{\nu 0} . \tag{10.11}$$

Here, the quantization volume initially contains the chromophore and two photons of the incident radiation; the factor of $q_2^{1/2} \equiv [q(q-1)]^{1/2}$ correspondingly arises from the successive operations of the photon annihilation operator. The above expression exploits the symmetry of the electric polarisation terms $e_i^{(\eta)}e_j^{(\eta)}$ with respect to exchange of the indices i and j. The second rank molecular response tensor $\alpha_{(ij)}^{\nu 0}$ is duly defined as:

$$\alpha_{(ij)}^{\nu 0} = -\frac{1}{2}\sum_r (E_{r0} - \hbar c p)^{-1}\left(\mu_i^{\nu r}\mu_j^{r0} + \mu_j^{\nu r}\mu_i^{r0}\right) , \tag{10.12}$$

where $E_{rs} = E_r - E_s$ is an energy difference between molecular states. The two dipole product contributions in the above expression relate to each of the possible time-orderings in which the two, indistinguishable input photons can be annihilated; the factor of $\frac{1}{2}$ is introduced to preclude over-counting, and bracketed subscripts denote symmetry with respect to interchange of the enclosed indices. In cases where the electronic level accessed by two-photon absorption equates to that from which subsequent radiative decay occurs, i.e. $\nu = \alpha$, it is prudent to allow the two-level approximation for the two-photon absorbing chromophore [36]. The tensor that determines the two-photon absorption properties of such a system then reduces to a form that features both static and transition dipoles, the former expressed as a shift in dipole moment that accompanies the transition:

$$\alpha_{(ij)}^{\alpha 0(TLA)} = -\frac{1}{2}(E_{\alpha 0} - \hbar c p)^{-1}\left(d_i \mu_j^{\alpha 0} + d_j \mu_i^{\alpha 0}\right). \tag{10.13}$$

By combining Eqs. (10.9) and (10.11), the following expression represents the output signal resulting from two-photon induced fluorescence:

$$I_{\text{flu}}^{(2)}(\phi) = \sum_{\xi} K^{(2)} \langle S_{(ij)k} \overline{S}_{(lm)n} T_{(ij)k} \overline{T}_{(lm)n} \rangle, \tag{10.14}$$

Here, the electric vector and molecular transition moment products are expressed as third rank tensors such that $S_{(ij)k}$ and $\overline{S}_{(ij)k}$ correspond to $e_i^{(\eta)} e_j^{(\eta)} \overline{e}_k^{(\eta')}$ and $\overline{e}_i^{(\eta)} \overline{e}_j^{(\eta)} e_k^{(\eta')}$, whilst $T_{(ij)k}$ and $\overline{T}_{(ij)k}$ signify $\alpha_{(ij)}^{\nu 0} \mu_k^{0\alpha}$ and $\overline{\alpha}_{(ij)}^{\nu 0} \overline{\mu}_k^{0\alpha}$ respectively. In this case, for an oriented sample, the dependence on emission angle is again $\cos^2\theta$. However the dependence on input polarization is considerably more intricate, being determined by a weighted combination of $\cos^2$ functions for each angle between the input polarization vector and one of a number of transition moments, i.e. $\boldsymbol{\mu}^{\nu r}$, $\boldsymbol{\mu}^{r0}$, for each level r.

For *three-photon* induced fluorescence, the transition between the ground and excited state of the chromophore, which requires the concerted absorption of an additional photon, progresses through two distinct virtual intermediate states. Substitution of Eqs. (10.3) and (10.4) into (10.1) where $n = 3$ yields the following matrix element cast in terms of a third rank molecular response tensor $\beta_{(ijk)}^{\nu 0}$:

$$M_{\nu 0}^{(3)}(\xi) = -q_3^{1/2} i \left(\frac{\hbar c p}{2\varepsilon_0 V}\right)^{\frac{3}{2}} e_i^{(\eta)} e_j^{(\eta)} e_k^{(\eta)} \beta_{(ijk)}^{\nu 0}. \tag{10.15}$$

As with the case of second rank tensor used to describe two-photon absorption, $\beta_{(ijk)}^{\nu 0}$ features a sum of dipole product contributions that account for all possible time-orderings of the identical input photons. Including a factor of $\frac{1}{6}$, again to offset over-counting, this third-rank molecular response tensor is defined thus:

$$\beta^{\nu 0}_{(ijk)} = \frac{1}{6}\sum_{r,s}\left[(E_{r0} - \hbar c\, p)(E_{s0} - 2\hbar c\, p)\right]^{-1} \left(\mu_i^{\nu s}\mu_j^{sr}\mu_k^{r0} + \mu_i^{\nu s}\mu_k^{sr}\mu_j^{r0} + \mu_j^{\nu s}\mu_i^{sr}\mu_k^{r0} + \mu_j^{\nu s}\mu_k^{sr}\mu_i^{r0} + \mu_k^{\nu s}\mu_i^{sr}\mu_j^{r0} + \mu_k^{\nu s}\mu_j^{sr}\mu_i^{r0}\right). \tag{10.16}$$

As with two-photon absorption, it is again expedient to re-express this general three-photon tensor in a more specific two-level form:

$$\beta^{\alpha 0}_{(ijk)} = \frac{1}{3}(E_{\alpha 0} - \hbar c\, p)^{-1}\Big[(E_{\alpha 0} - 2\hbar c\, p)^{-1}\left(\mu_i^{\alpha 0} d_j d_k + \mu_j^{\alpha 0} d_k d_j + \mu_k^{\alpha 0} d_i d_k\right) - (2\hbar c\, p)^{-1}\left(\mu_i^{\alpha 0}\mu_j^{0\alpha}\mu_k^{\alpha 0} + \mu_i^{\alpha 0}\mu_k^{0\alpha}\mu_j^{\alpha 0} + \mu_j^{\alpha 0}\mu_i^{0\alpha}\mu_k^{\alpha 0}\right)\Big]. \tag{10.17}$$

The fluorescence signal due to three-photon excitation can now be represented as:

$$I^{(3)}_{\text{flu}}(\phi) = \sum_{\xi} K^{(3)}\left\langle S_{(ijk)l}\overline{S}_{(mno)p}T_{(ijk)l}\overline{T}_{(mno)p}\right\rangle, \tag{10.18}$$

The electric polarization and molecular transition moments are described in terms of fourth rank tensors, where $S_{(ijk)l}$ and $\overline{S}_{(ijk)l}$ respectively represent $e_i^{(\eta)}e_j^{(\eta)}e_k^{(\eta)}\overline{e}_l^{(\eta')}$ and $\overline{e}_i^{(\eta)}\overline{e}_j^{(\eta)}\overline{e}_k^{(\eta)}e_l^{(\eta')}$, whilst $T_{(ijk)l}$ and $\overline{T}_{(ijk)l}$ correspond to $\beta^{\nu 0}_{(ijk)}\mu_l^{0\alpha}$ and $\overline{\beta}^{\nu 0}_{(ijk)}\overline{\mu}_l^{0\alpha}$, the final index of each again being associated with the one-photon emission. The orientation relative to the input polarization again depends on a multitude of angles, corresponding in this case to the orientations of the transition moments $\boldsymbol{\mu}^{\nu s}$, $\boldsymbol{\mu}^{sr}$, $\boldsymbol{\mu}^{r0}$, summed over states r and s.

10.3.3 Freely Tumbling Molecules

The general results presented so far for the fluorescence output in one-, two- and three-photon induced systems are applicable to systems in which the responsible chromophores have arbitrary orientations with respect to experimentally determined input and detection configurations. As such, the derived expressions are already directly applicable to all ordered samples in which individual chromophores are held in a fixed orientation. To address disordered systems it is expedient to secure corresponding results for an opposite extreme – systems of completely random dipole orientation, which represents a set of freely tumbling molecules. To this end, the above results can be subjected to an established, integration free, orientational averaging protocol utilizing isotropic tensors [37–39].

Beginning with the signal for *one-photon* induced fluorescence, Eq. (10.10) exhibits a sum over four separate Cartesian indices. By first uncoupling the molecular and radiation components of the system – achieved by assigning the former to a

molecule-fixed frame of reference and the latter to a laboratory-fixed equivalent – and then performing a fourth-rank average, tensor contractions are effected. All of the ensuing results are then expressible in terms of scalar products between input and output polarization components. In the commonly utilized deployment of plane-polarized input laser light, the polarization vectors are real and the scalar product of any two is concisely summarized by:

$$\overset{(-)(\eta)}{\mathbf{e}} \cdot \overset{(-)(\eta')}{\mathbf{e}} = \delta_{\eta\eta'} + \left(1 - \delta_{\eta\eta'}\right) \cos\phi \,, \tag{10.19}$$

where ϕ is the angle between the input and output polarization vectors. The final result for the orientationally averaged fluorescence output emerges in terms of ϕ as;

$$I^{(1)}_{\text{flu}}(\phi) = \frac{K^{(1)}}{30}\left[\left(T_{\lambda\lambda}\overline{T}_{\mu\mu} + T_{\lambda\mu}\overline{T}_{\mu\lambda}\right)\left(3\cos^2\phi - 1\right) - \left(2T_{\lambda\mu}\overline{T}_{\lambda\mu}\right)\left(\cos^2\phi - 2\right)\right], \tag{10.20}$$

involving three molecular invariants, $T_{\lambda\lambda}\overline{T}_{\mu\mu}$, $T_{\lambda\mu}\overline{T}_{\mu\lambda}$ and $T_{\lambda\mu}\overline{T}_{\lambda\mu}$ – whose form and means of characterization, using linear and circular polarizations, were first identified in pioneering work by McClain [40, 41]. For this case of one-photon induced fluorescence, it is further possible to express the molecular tensors in Eq. (10.20) relative to the magnitude of the molecular transition moments $\boldsymbol{\mu}^{\nu 0}$ and $\boldsymbol{\mu}^{0\alpha}$, and the angle between them, β, such that:

$$I^{(1)}_{\text{flu}}([\phi],[\beta]) = \frac{K^{(1)}\left|\boldsymbol{\mu}^{\nu 0}\right|^2\left|\boldsymbol{\mu}^{0\alpha}\right|^2}{30}\left[\left(3\cos^2\phi - 1\right)\left(2\cos^2\beta\right) - 2\left(\cos^2\phi - 2\right)\right], \tag{10.21}$$

where the identities $T_{\lambda\lambda}\overline{T}_{\mu\mu} = T_{\lambda\mu}\overline{T}_{\mu\lambda} = \left|\boldsymbol{\mu}^{\nu 0}\right|^2\left|\boldsymbol{\mu}^{0\alpha}\right|^2\cos^2\beta$, and $T_{\lambda\mu}\overline{T}_{\lambda\mu} = \left|\boldsymbol{\mu}^{\nu 0}\right|^2 \left|\boldsymbol{\mu}^{0\alpha}\right|^2$ apply. Resolving Eq. (10.21) for fluorescence components parallel or perpendicular to the input polarization leads to the familiar degree of *fluorescence anisotropy* for a randomly oriented sample [21, 22].

To resolve the corresponding anisotropy equations for two- and three-photon induced fluorescence invokes identical methods based on sixth- and eighth-rank averages [42], respectively. From a detailed analysis of the results, it emerges that the equations determining the multiphoton fluorescence response prove expressible in a relatively simple, generic form:

$$I^{(n)}_{\text{flu}}(\phi) = K^{(n)}\left[\Lambda^{(n)}\left(3\cos^2\phi - 1\right) - \Upsilon^{(n)}\left(n\cos^2\phi - (n+1)\right)\right], \tag{10.22}$$

with both $\Lambda^{(n)}$ and $\Upsilon^{(n)}$ each representable as a sum of distinct molecular invariants. While the detailed form of such invariants is reported elsewhere [43], it should be noted that an inherent summation in each over accessible virtual intermediate states

precludes the possibility of further simplifying the above result by attempting to factorize out the absorption and emission transition moments, as was achieved for Eq. (10.21), without introducing further assumptions that would compromise the generality of the outcome.

These generic results represent tools that can be applied in the analysis of polarization-determined features in two- and three-photon fluorescence from samples of considerable molecular complexity. By determining how either type of multiphoton-induced fluorescence signal responds to the orientation of a polarizer, it is in principle possible to distinguish and quantify any departure from local orientational order or disorder within a bulk sample. Key to this discrimination is the difference in angular disposition of the fluorescence polarization. In samples whose chromophores are rigidly oriented, the fluorescence signal from an ensemble with common orientation takes the form of a $\cos^2$ distribution with respect to the angle θ between the emission moment and the resolved polarization. On rotation of the polarizer through 180° there will be an angle at which the signal is extinguished – both for single- and multi-photon induced fluorescence. However, as will be shown, the behaviour from a randomly oriented sample is in general distinctively different.

To proceed, it is helpful to cast the general result that determines the multiphoton fluorescence signal, in the following form:

$$I_{\mathrm{flu}}^{(n)}(\phi) = K'^{(n)}\left[n + 1 - y + (3y - n)\cos^2\phi\right], \tag{10.23}$$

where $K'^{(n)} = K^{(n)}\Upsilon^{(n)}$, $y = \Lambda^{(n)}/\Upsilon^{(n)}$. The latter parameter is a scalar that characterizes the relative values of the molecular invariant groupings in Eq. (10.22). Although the precise value of y will depend on the component values of the transition tensors, it can be shown that it is positive and limited to an upper bound of $(n+1)$. Figure 10.1 exhibits the functional form of the fluorescence polarization, for single-photon induced fluorescence, over the range $(0 \le \phi \le \pi/2)$ – results of identical form but different scale have also been recorded for the multiphoton processes. Each graph shows the behavior for different values of y; the "magic angle condition" represented as the point at which the curves for all different values of y intersect. The curve for $3y/n = 0.1$, for example, represents an extreme condition, $\Lambda^{(n)} \ll \Upsilon^{(n)}$, characterized by strongly depolarized emission. On the other hand the case $3y/n = 1.0$ is of special interest because the fluorescence proves to be independent of the resolving polarization, thus representing a condition under which the fluorescence produced through the concerted absorption of any number of photons becomes completely unpolarized.

Results for $3y/n = 3.0$ are perhaps the most interesting, being indicative of the statistically most likely outcome. This condition arises when, within the general result, all featured molecular invariants are of approximately equal value. It is remarkable that this condition leads in every case to $\Lambda^{(n)}/\Upsilon^{(n)} = y = n$. Here, there is a strong retention of polarization, the corresponding emission anisotropies $r = (I_{\parallel} - I_{\perp})/(I_{\parallel} + 2I_{\perp})$ proving to conform to the simple formula

$r = 2n/(2n+3)$ and yielding the following specific values: (i) $n = 1$; $r = 2/5 = 0.4$, the familiar one-photon result; [21] also (ii) for two-photon excitation, $n = 2$; $r = 4/7 = 0.57$; (iii) for the three-photon case $n = 3$; $r = 6/9 = 0.67$. These limiting results are in precise agreement with the values that arise specifically when all transition moments are considered parallel, a special case originally considered and reported by Lakowicz et al. [44]

The correlation serves to verify a limiting case of the present, more general results – but it is also notable that the conditions under which such behavior arises are not only associated with parallel transition moments. The same observations will result, for example, if all of the molecular transition tensor elements have similar values. In conclusion, the considered cases all satisfy the condition that the ratio of maximum and minimum fluorescence intensities $I^{(n)}_{\min}/I^{(n)}_{\max}$ lies in the interval $[0,\ 1/(2n+1)]$. It is worth recalling that rotation of the resolving polarizer can entirely extinguish the fluorescence from an orientationally perfectly ordered sample or domain. This suggests that in a general case the measured value of $I^{(n)}_{\min}/I^{(n)}_{\max}$ registered against the scale $[0,\ 1/(2n+1)]$ should represent a robust, easily determined single-value indicator of the degree of disorder in fluorescence produced by n-photon excitation.

10.4 Laser-Controlled Fluorescence

Using the same quantum formalism, a completely novel development in relation to fluorescence is now to be discussed. Its background is the well-known fact that the throughput of a laser beam into a photo-activated system may produce stimulated emission when the laser frequency matches the fluorescence energy – a phenomenon that has found analytical applications, for example, in the recently Nobel Prize winning technique of stimulated emission depletion spectroscopy [45–51]. However, outside of stimulated emission, it has further emerged that a moderately intense, *off*-resonant laser beam may significantly alter the rate and intensity of fluorescence [52–55]. Under these circumstances, the probe laser essentially confers optical nonlinearity onto the fluorescent emission – and consequently, each excited-state lifetime is appreciably modified. One may draw analogies with the well-known enhancement of optical emission through its coupling with a plasmonic surface [56–65]. However, this novel development modifies spontaneous fluorescent emission through direct interaction with the oscillating electric field of throughput radiation, without the presence of any surface. With initial estimates suggesting that conventional fluorescence lifetimes could be reduced by 10 % or more [52], for input beam intensities in the 10^{15} W m^{-2} range, such a prospect is readily amenable to measurement with modulation-based instrumentation – and it also affords a new means of exerting control over the fluorescence process.

In the following summary of theory, the effects of laser – controlled emission on fluorescence anisotropy are determined for a system of randomly oriented chromophores. It is also shown that a two-level formulation of theory leads to relatively tractable expressions with a broad validity extending from quantum dots [11, 12, 14] to fluorescent proteins [13, 15–18] – indeed any material whose emission spectrum is dominated by one excited electronic state. A limiting case is then considered in which fluorescence arises solely through activation by the off – resonant input. First, outside of these two – level considerations, the mechanism of laser-controlled fluorescence is to be more fully described.

10.4.1 The Mechanism

We first return to the well-established tenet that the theory of single-photon emission from any individual chromophore, since it involves a single matter-radiation interaction, is cast in terms of first – order time-dependent perturbation theory. In cases where no other light is present – as is the case in normal experiments, once the radiation responsible for initial electronic excitation has traversed the system – then higher order (odd-rank) perturbation terms are insignificant, and only denote self-energy corrections. However, higher-order interactions of much greater significance can occur on the application of an off-resonant probe laser, *i.e.* a beam whose wavelength lies within a transparent region of the chromophore. Although no net absorption or stimulated emission of the beam then occurs, elastic forward-scattering events are present – namely, photons are annihilated and created into the same radiation mode (the latter photon emerging as if unchanged from the former). Through nonlinear coupling, such events may directly engage with the fluorescent emission in a mechanism comprising *three* concerted matter-radiation interactions (Fig. 10.2), *i.e.* a process that has to be described using third-order perturbation theory. In passing, it is noteworthy that the off-resonant probe beam produces similar effects in connection with resonance energy transfer [66–68] (Fig. 10.3). AU1

The intensity of fluorescence $I'(\Omega')$ (or power per unit solid angle) is determined by multiplying the Fermi Rule of Eq. (10.5) by the energy of a fluorescent photon, $\hbar\omega' \equiv \hbar c k'$ [69, 70], and it signifies the single-molecule fluorescence signal that follows relaxation from the relevant excited state. By including laser-controlled fluorescence, the net intensity is found from $I'(\Omega')\mathrm{d}\Omega' = 2\pi\rho c k' \left| M_{\mathrm{flu}}^{(1)} + M_{\mathrm{flu}}^{(3)} \right|^2$, where $M_{\mathrm{flu}}^{(1)}$ and $M_{\mathrm{flu}}^{(3)}$ are the quantum amplitudes for first – and third – order fluorescent processes, respectively, and the density of radiation states is $\rho = \left(k'^2 V / 8\pi^3 \hbar c\right)\mathrm{d}\Omega'$. As determined elsewhere [53], the following general result is derived from this Fermi-related expression;

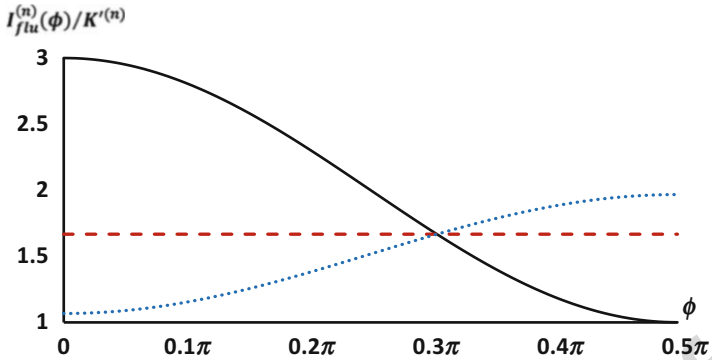

Fig. 10.2 Angular disposition of polarization in fluorescence produced by single-photon absorption ($n = 1$): *blue* (*dotted*) curve $3y/n = 0.1$; *red* (*dashed*) curve $3y/n = 1$; *black* (*solid*) curve $3y/n = 3$

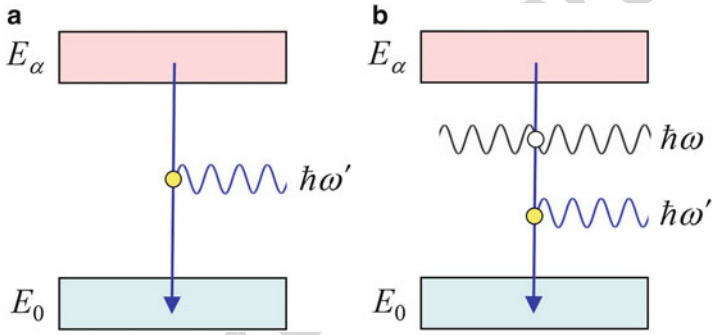

Fig. 10.3 Energy level representation for: (**a**) spontaneous and (**b**) nonlinear coupling mechanisms for fluorescence. Electronic states (and their vibrational manifolds) are signified by boxes, where E_0 and E_α are correspondingly the ground and excited molecular states. Wavy lines indicate photon propagation and the vertical arrow is a decay transition due to the emission. The emitted fluorescence has energy defined by $\hbar\omega'$, while photons of the off-resonant laser beam are of energy $\hbar\omega$. The yellow dot symbolizes a single matter-radiation interaction and the white dot represents two such interactions (i.e. elastic forward-scattering)

$$I'(\Omega') = \left(\frac{ck'^4}{8\pi^2\varepsilon_0}\right)\Big[e'_i e'_j \mu_i^{0\alpha}\overline{\mu}_j^{0\alpha} + (I/c\varepsilon_0)e_i e_j e'_k e'_l \chi_{ijk}^{0\alpha}(\omega';-\omega,\omega)\overline{\mu}_l^{0\alpha} + (I^2/4c^2\varepsilon_0^2)e_i e_j e'_k e_l e_m e'_n \chi_{ijk}^{0\alpha}(\omega';-\omega,\omega)\overline{\chi}_{lmn}^{0\alpha}(\omega';-\omega,\omega)\Big], \tag{10.24}$$

where I is the irradiance of the laser probe, and **e** now represents the polarization vector of the probe, off-resonant photons with energy $\hbar ck$. The first term corresponds to spontaneous emission, intrinsic to the system and independent of the probe laser beam, while the last term signifies a coupling of the elastically forward – scattered probe beam with the fluorescence emission. The middle term, linear in I,

signifies a quantum interference of these two concurrent processes. In general, it is assumed that the leading term in Eq. (10.24) is non – zero and the second one is the leading correction – although a circumstance can be arise in which solely the third term exists, *i.e.* when the first and second terms are null (this is discussed in Sect. 10.4.3). Continuing, the sum-over-states form of the third-order nonlinear optical 'transition hyperpolarizability' tensor $\chi^{0\alpha}_{ijk}\left(\omega';-\omega,\omega\right)$, explicitly exhibiting the frequency dispersion, is as follows;

$$\begin{aligned}\chi^{0\alpha}_{ijk}\left(\omega';-\omega,\omega\right) &= \sum_{r}\sum_{s\neq\alpha}\left(\frac{\mu^{0s}_{k}\mu^{sr}_{j}\mu^{r\alpha}_{i}}{\widetilde{E}_{s\alpha}\left(\widetilde{E}_{r\alpha}-\hbar\omega\right)}+\frac{\mu^{0s}_{k}\mu^{sr}_{i}\mu^{r\alpha}_{j}}{\widetilde{E}_{s\alpha}\left(\widetilde{E}_{r\alpha}+\hbar\omega\right)}\right)\\ &+\sum_{r}\sum_{s}\left(\frac{\mu^{0s}_{j}\mu^{sr}_{k}\mu^{r\alpha}_{i}}{\left(\widetilde{E}_{s\alpha}-\hbar\omega+\hbar\omega'\right)\left(\widetilde{E}_{r\alpha}-\hbar\omega\right)}+\frac{\mu^{0s}_{i}\mu^{sr}_{k}\mu^{r\alpha}_{j}}{\left(\widetilde{E}_{s\alpha}+\hbar\omega+\hbar\omega'\right)\left(\widetilde{E}_{r\alpha}+\hbar\omega\right)}\right)\\ &+\sum_{r\neq 0}\sum_{s}\left(\frac{\mu^{0s}_{j}\mu^{sr}_{i}\mu^{r\alpha}_{k}}{\left(\widetilde{E}_{s\alpha}-\hbar\omega+\hbar\omega'\right)\left(\widetilde{E}_{r\alpha}+\hbar\omega'\right)}+\frac{\mu^{0s}_{i}\mu^{sr}_{j}\mu^{r\alpha}_{k}}{\left(\widetilde{E}_{s\alpha}+\hbar\omega+\hbar\omega'\right)\left(\widetilde{E}_{r\alpha}+\hbar\omega'\right)}\right).\end{aligned} \tag{10.25}$$

The tildes serve as a reminder to add to the excited state energies, in the case of near-resonance conditions, imaginary terms to accommodate line-shape and damping. With reference to later comments, it is worth noting here that there is no assumption of Kleinman symmetry [71] at this stage – this being a simplifying device, commonly made for calculational expediency that would impose complete index symmetry for such a tensor.

Considering the dependence of the fluorescence signal on the optical frequency of the probe, it is evident that the denominators within the transition hyperpolarizability tensor of Eq. (10.25) have an important role in determining any degree of enhancement or suppression of the fluorescence emission. These factors are dependent on the relative spacing of the chromophore energy levels relative to the magnitude of the probe photon energy. It is convenient to assume that the probe light is delivered in the form of a tunable beam with optical frequency $\omega < \omega'$, a condition that specifically precludes single-photon excitation of ground-state molecules. It will also be assumed that the chosen range of probe frequencies cannot produce multiphoton excitation.

The main challenge in evaluating the nonlinear response characterized by the transition tensors within Eq. (10.24) now lies with implementing the required sum over intermediate states. As mentioned earlier, it is fully justifiable to consider only states in which the majority of the optical transitions occur, *i.e.* to employ a two-state model. Limiting the intermediate states of Eq. (10.25) to just $|0\rangle$ and $|\alpha\rangle$ restricts the transition sequences from excited to ground states that progress through r and s. Applying the prescription described in Sect. 10.2 to the six terms of

Eq. (10.25) produces a two-level hyperpolarizability tensor that is generally expressible as a sum of twelve separate contributions. Further simplification ensues because a number of these terms, for which $r = 0$ and/or $s = \alpha$, are precluded by the conditions of perturbation theory, namely the exclusion of virtual states that equate to the initial or final state. The two-state form of $\chi^{0\alpha}_{ijk}\left(\omega';-\omega,\omega\right)$ thus re-emerges as: [55]

$$\chi^{0\alpha}_{ijk}\left(\omega';-\omega,\omega\right) = \frac{2}{\hbar^2}\frac{\mu^{0\alpha}_j\mu^{0\alpha}_k\mu^{0\alpha}_i}{\left(\omega^2-\omega'^2\right)} + \frac{\mu^{0\alpha}_j d_i d_k}{\hbar^2\omega\omega'} - \frac{\mu^{0\alpha}_i d_j d_k}{\hbar^2\omega\omega'} \quad . \tag{10.26}$$

It may be observed that the second and third terms on the right in Eq. (10.26) exhibit an antisymmetry with respect to interchange of the indices i and j. However, in the physical observable delivered by Eq. (10.24), this tensor is index-contracted with a i,j-symmetric product of polarization vectors. Consequently, since only the i,j-symmetric part of Eq. (10.26) can contribute to the fluorescence signal, it is expedient to replace $\chi^{0\alpha}_{ijk}\left(\omega';-\omega,\omega\right)$, without further approximation, by an index-symmetrised form, $\chi^{0\alpha}_{(ij)k}\left(\omega';-\omega,\omega\right)$ that is defined as follows:

$$\chi^{0\alpha}_{(ij)k}\left(\omega';-\omega,\omega\right) \equiv \frac{1}{2}\left(\chi^{0\alpha}_{ijk}\left(\omega';-\omega,\omega\right) + \chi^{0\alpha}_{jik}\left(\omega';-\omega,\omega\right)\right) = \frac{2}{\hbar^2}\frac{\mu^{0\alpha}_i\mu^{0\alpha}_j\mu^{0\alpha}_k}{\left(\omega^2-\omega'^2\right)} . \tag{10.27}$$

It is notable that the expression on the right is, in fact, fully index-symmetric, therefore the two-level model delivers a result that is consistent with the adoption of Kleinman symmetry – even though the latter condition (a simplification that is often effected in other realms of nonlinear optics) has not been artificially imposed. Furthermore, there is a significant physical consequence; it emerges that the mechanism for the laser-controlled emission depends only on the transition dipole, and not on the static moments.

10.4.2 Effects of the Probe Beam on the Fluorescence Anisotropy

As discussed earlier, a great deal of information that is highly relevant to speciation and structure determination can be derived from fluorescence anisotropy. Specifically, the anisotropy parameters normally signify the degree to which fluorescence retains a directionality of polarization from the initial excitation – see for example chapter 7 of the classic text by Valeur [22]. The associated experimental measurements can also inform on excited state photophysical processes such as internal conversion, hindered rotation, rotational diffusion, intramolecular energy transfer

etc. Each of these processes represents one means by which the fluorescent emission can exhibit properties quite different from the preceding absorption – quite apart from the Stokes shift in wavelength that is normally apparent. The former processes all provide situations in which the emission dipole moment need not be parallel to the absorption moment. To accommodate such features in the present theory, the initial absorption must again be incorporated into our analysis. Since the probe beam is only delivered to the system after the initial excitation, we have:

$$\left\langle I'\left(\Omega'\right)\right\rangle \sim \left\langle \left|M^{(1)}_{\text{abs}}\right|^2 \left|M^{(1)}_{\text{flu}} + M^{(3)}_{\text{flu}}\right|^2 \right\rangle, \tag{10.28}$$

an expression established under identical conditions, regarding the separation of excitation and emission processes, as was employed in the derivation of the fluorescent signal presented earlier as Eq. (10.7). The anisotropy is now determined from the general expression $r' = \left(\left\langle I'_{\parallel}\right\rangle - \langle I'_{\perp}\rangle\right) / \left(\left\langle I'_{\parallel}\right\rangle + 2\langle I'_{\perp}\rangle\right)$, where $\left\langle I'_{\parallel}\right\rangle$ and $\langle I'_{\perp}\rangle$ are the components of fluorescence intensity polarized parallel and perpendicular, respectively, to the electric polarization vector of the initial excitation beam – the initial absorption is proportional to $\mathbf{e}_0 \cdot \boldsymbol{\mu}^{\nu 0}$, where $\mathbf{e}_0$ represents the input polarization vector aligned by definition to the z – direction.

For initial purposes it is assumed, as will often be the case, that the third contribution to the fluorescence signal in Eq. (10.24) is negligibly small. Duly considering the first two terms, the rotationally averaged fluorescence output from a two-level molecular system is determined and can be expressed as follows, explicitly cast in terms of the three distinct angles between each pair of polarization vectors, for the incident, off-resonant probe and emitted light: $\theta = \cos^{-1}(\mathbf{e}_0 \cdot \mathbf{e})$, $\varphi = \cos^{-1}\left(\mathbf{e} \cdot \mathbf{e}'\right)$ and $\phi = \cos^{-1}\left(\mathbf{e}_0 \cdot \mathbf{e}'\right)$:

$$\begin{aligned}\left\langle I'\left(\Omega'\right)\right\rangle = \; & K^{(1)}\big[T_{ii}\overline{T}_{jj}(3\cos^2\phi - 1) + T_{ij}\overline{T}_{ij}(-\cos^2\phi + 2) \\ & + \frac{I}{7c\varepsilon_0}\big(T_{i(ijj)}\overline{T}_{kk}\left(6\cos\theta\cos\varphi\cos\phi - 2\cos^2\theta - 2\cos^2\varphi + 5\cos^2\phi - 1\right) \\ & + T_{i(ijk)}\overline{T}_{jk}(6\cos\theta\cos\varphi\cos\phi + 5\cos^2\theta - 2\cos^2\varphi - 2\cos^2\phi - 1) \\ & + T_{i(jjk)}\overline{T}_{ik}(-4\cos\theta\cos\varphi\cos\phi - \cos^2\theta + 6\cos^2\varphi - \cos^2\phi + 3)\big)\big].\end{aligned} \tag{10.29}$$

In this expression, the first two terms signifying the expected response have a form identical to Eq. (10.20) under the condition that $T_{\lambda\lambda}\overline{T}_{\mu\mu} = T_{\lambda\mu}\overline{T}_{\mu\lambda}$, which is always true under the standard assumption that the inherent electric dipole moments are real.

The higher order contributions in the above Eq. (10.29) represent the lead corrections produced by the probe laser. The expression continues the established shorthand notation that represents transition moment products in terms of second- and fourth-rank molecular tensors, within each of which the first index is associated with the initial molecular excitation. In deriving specific results for independent

polarization components, further simplification can be achieved by writing each of the above molecular tensors explicitly in terms of components of the two transition dipole moments, the photo-selected $\boldsymbol{\mu}^{\nu 0}$ and the emission $\boldsymbol{\mu}^{0\alpha}$. Following the introduction of β as the angle between these two dipoles, the fluorescence is readily resolved for polarizations $\mathbf{e}'$ in the z – and x-directions, respectively. The results are given as follows for $\phi = 0$, $\varphi = \pi/2$, $\theta = \pi/2$;

$$\left\langle I'_{\parallel}\left(\Omega'\right)\right\rangle = K^{(1)}\left|\boldsymbol{\mu}^{0\alpha}\right|^2\left|\boldsymbol{\mu}^{\nu 0}\right|^2\left[2\cos^2\beta + 1 + \frac{I\left|\boldsymbol{\mu}^{0\alpha}\right|^2(\cos^2\beta + 2)}{7\varepsilon_0\hbar^2 c\left(\omega^2 - \omega'^2\right)}\right], \tag{10.30}$$

and for $\phi = \pi/2$, $\varphi = 0$, $\theta = \pi/2$:

$$\left\langle I'_{\perp}\left(\Omega'\right)\right\rangle = K^{(1)}\left|\boldsymbol{\mu}^{0\alpha}\right|^2\left|\boldsymbol{\mu}^{\nu 0}\right|^2\left[2 - \cos^2\beta + \frac{3I\left|\boldsymbol{\mu}^{0\alpha}\right|^2(3 - 2\cos^2\beta)}{7\varepsilon_0\hbar^2 c\left(\omega^2 - \omega'^2\right)}\right]. \tag{10.31}$$

Hence, upon substitution of Eqs. (10.30) and (10.31) into the general anisotropy expression, it is found that:

$$r' = \frac{3\cos^2\beta - 1 + KI\left|\boldsymbol{\mu}^{0\alpha}\right|^2(\cos^2\beta - 1)}{5 + KI\left|\boldsymbol{\mu}^{0\alpha}\right|^2(20 - 11\cos^2\beta)/7}, \tag{10.32}$$

where $K = \left(\varepsilon_0\hbar^2 c\left(\omega^2 - \omega'^2\right)\right)^{-1}$. In the limiting case $I = 0$ the well – known expression [22] $r' = (1/5)(3\cos^2\beta - 1)$ for conventional fluorescence is recovered. Generally, however, a change in fluorescence anisotropy will be apparent due to the interaction with the probe beam – even though the radiation state of the probe laser beam is unaltered.

10.4.3 Configuration for higher order effects

Up until now, the nonlinear contribution to the fluorescence output (the I^2 quadratic term) has not been considered in detail. Nevertheless, there are circumstances in which such a term alone provides the fluorescence response, *i.e.* when the first and second terms of Eq. (10.24) are null. Addressing such a case requires progression beyond the two-level approximation, so that higher energy levels are accommodated. Consider, for instance, a system where (following optical excitation) the electronic population is efficiently transferred to a state $|\alpha\rangle$ that would normally decay non-radiatively, if transitions from $|\alpha\rangle$ to $|0\rangle$ are weak or entirely precluded – as, for example, through inherent geometric or symmetry constraints. In such a situation, terms that feature the transition dipole $\boldsymbol{\mu}^{0\alpha}$ in Eq. (10.24) do not

contribute: radiative emission only occurs in a response to the off-resonant throughput beam, in a three-photon allowed transition.

Such a configuration may provide the basis for an all-optical molecular switch, whose operation would be as follows: (i) a molecule is indirectly excited to a 'dark' state (*i.e.* one whose direct dipolar excitation from the ground state is forbidden); (ii) precluded by the one-photon dipole selection rules, fluorescence from the 'dark' state occurs on application of the probe beam only; (iii) this activation of the emission occurs for molecular transitions that are three – photon allowed, but single-photon forbidden – examples are afforded by excited states of A_2 symmetry, in molecules of C_{2v} or C_{3v} symmetry, or states of A_u symmetry in D_{2h} species. In summary, switching action occurs since the throughput and absence of the input laser results in activation and deactivation of the fluorescence, respectively. Practically, it will be necessary for the radiation to be delivered in a pulse whose duration and delay, both with respect to the initial excitation, are sufficiently short that it can engage with the system before there is significant non – radiative dissipation of the excited state. For fluorescence output of this type, an eighth-rank rotational average will lead to the following expression:

$$\begin{aligned}\langle I'(\Omega')\rangle = \left(\frac{I^2}{84c^2\varepsilon_0{}^2}\right)K^{(1)}\big[&3T_{i(ijj)}\overline{T}_{k(kll)}(3\cos^2\theta\cos^2\varphi - \cos^2\theta - \cos^2\varphi + \cos^2\phi)\\ &+6T_{i(ijk)}\overline{T}_{j(kll)}(6\cos\theta\cos\varphi\cos\phi - \cos^2\theta - 2\cos^2\varphi - 2\cos^2\phi + 1)\\ &+3T_{i(ijk)}\overline{T}_{l(jkl)}(\cos^2\theta\cos^2\varphi - 4\cos\theta\cos\varphi\cos\phi + 5\cos^2\theta + \cos^2\varphi + 4\cos^2\phi - 3)\\ &+3T_{i(jjk)}\overline{T}_{i(kll)}(-\cos^2\theta\cos^2\varphi - 4\cos\theta\cos\varphi\cos\phi + \cos^2\theta + 5\cos^2\varphi + \cos^2\phi - 1)\\ &+T_{i(jkl)}\overline{T}_{i(jkl)}(-\cos^2\theta\cos^2\varphi + 4\cos\theta\cos\varphi\cos\phi - 5\cos^2\theta + \cos^2\varphi - 4\cos^2\phi + 7)\big].\end{aligned} \tag{10.33}$$

Here, the **T** tensors accommodate summation over products of transition dipole moments that specifically exclude $\boldsymbol{\mu}^{0\alpha}$, since decay transitions are symmetry-forbidden under one – photon selection rules. However, for simplicity, we retain the assumption of Kleinman index symmetry in the embedded $\boldsymbol{\chi}$ tensor (corresponding to the last three indices in each **T**).

For completeness, one may determine an entirely general result for the laser-modified fluorescence anisotropy. Such an expression accommodates all the terms of Eq. (10.24), including the higher-order contributions that are usually negligible (outside of the mentioned model), and is given by:

$$r' = \frac{3\cos^2\beta - 1 + KI\left|\boldsymbol{\mu}^{0\alpha}\right|^2(\cos^2\beta - 1) + \left(K^2I^2\left|\boldsymbol{\mu}^{0\alpha}\right|^4/21\right)(15\cos^2\beta - 17)}{5 + \left(KI\left|\boldsymbol{\mu}^{0\alpha}\right|^2/7\right)(20 - 11\cos^2\beta) + \left(K^2I^2\left|\boldsymbol{\mu}^{0\alpha}\right|^4/21\right)(43 - 30\cos^2\beta)}. \tag{10.34}$$

In cases where the absorption and emission transition moments are parallel or anti-parallel, we may then secure the simpler result:

$$r' = \frac{42 - 2K^2I^2\left|\boldsymbol{\mu}^{0\alpha}\right|^4}{105 + 27KI\left|\boldsymbol{\mu}^{0\alpha}\right|^2 + 13K^2I^2\left|\boldsymbol{\mu}^{0\alpha}\right|^4}. \tag{10.35}$$

With increasing intensity of the probe beam, the first departures from the laser-free result, $r' = 0.4$, can be anticipated in the linear-response regime. In fact, it is evident from Taylor series expansions of both Eqs. (10.34) and (10.35) that a plot of the measured anisotropy against I will exhibit a monotonic reduction taking the form $r' \approx \frac{1}{5}(3\cos^2\beta - 1)(1 - \eta I)$, whose constant of proportionality η can be interpreted in terms of the transition moments. Beyond the proposed model to optically switch 'on' and 'off' fluorescent emission using an off-resonance probe beam, the capacity to engage with and to optically control fluorescence also offers significant new grounds for the interrogation of fluorescent materials.

10.5 Multi-emitter Fluorescence

Until this point, fluorescence from an isolated single-molecule source has been considered. Whilst there are some imaging applications of fluorescence that resolve the emission of individual emitters, most fluorescence studies detect signals created through the uncorrelated emission from numerous fluorophores. Of course, optical processes can be appreciably modified by the presence of neighboring material – for example secondary co-doped chromophores – if they are in close proximity [72–75]. It is also known that plasmonic interactions of molecules coupled with a metallic nanoantenna may alter their rate of fluorescent emission [76–83]. However, in most fluorescence studies the net response from a system of emitters can be assumed to be representative of the mean signal from each component.

There are, nonetheless, conditions where such implicit reliance on the ergodic theorem fails at the quantum level, namely when two or more active fluorophores are cooperatively involved in each individual photon emission. To account for the effects of neighboring *molecules*, the focus of this section is the correlated fluorescence from molecular sources that experience mutual interactions. In contrast to the fluorescence phenomena considered in the previous sections, it is most appropriate for the emitters to now be considered immobile and locally correlated in position, as for example would be the case for fluorophores that are surface-adsorbed – or indeed surface-functionalized. Clearly, results will be dependent on the displacement of the detector from the emitter pair, the relative dipolar orientation of the detector with respect to the pair of emitters, and the coupling parameters of the nanoemitters and detector.

It transpires that novel electrodynamic mechanisms can operate between such electromagnetically coupled sources of emission. To begin, theory is developed for

fluorescent emission from a pair of nanoemitters, and the effect of a phase difference between the excited state wavefunctions of the pair is considered. This possibility, as will emerge, proves to be of substantial importance when the number of nanoemitters is greater than two. More specialized systems, involving three or more nanoemitters, then afford a basis for generating optical vortex radiation, *i.e.* a form of 'twisted' light that involves an azimuthal progression of phase around a singularity.

10.5.1 Emission from a Nanoemitter Pair

Consider a system in which two molecular nanoemitters A and B in close proximity are so placed that significant electromagnetic coupling occurs between them. There are three distinct types of fluorescence that can occur, in which this coupling can manifest features that differ from the fluorescence of either individual component: (a) single – photon emission from an individual excited molecule whose states are influenced by electromagnetic coupling with its neighbor; (b) single – photon excitonic emission from the pair, in which a single initial electronic excitation is delocalized across both molecules; (c) correlated two-photon emission from the pair, in which both emitters are initially electronically excited [84]. To fulfil the initial conditions for the latter, third case is experimentally more demanding, and the phenomenon also presents less novelty; accordingly, we here focus on the first two scenarios.

First, for case (a) we consider the effects of fluorescent emission of a photon of energy $\hbar\omega = \hbar ck$, from a molecule labelled A under the influence of coupling with a neighbor B. To correctly account for features in the near-field, where some of the most distinctive features can be expected to arise, it will be helpful to begin by considering the full system to comprise three elements, one of which is a light detector, D (Later, explicit reference to such a device is removed for simplicity.) The matrix element for this system is represented by:

$$M^A = M^{DA} + M^{DAB} + M^{DBA} + M^{BDA}. \tag{10.36}$$

Here, the excitation is localized on molecule A prior to emission, so that the leading term represents direct coupling (photon propagation) between A and the detector, independent of the second emitter. This case is more concisely expressed as:

$$M^{DA} = \mu_i^{\nu 0}(D) V_{ij}(k, \mathbf{R}_{DA}) \mu_j^{0\alpha}(A), \tag{10.37}$$

where $\mathbf{R}_{DA}$ is the displacement between D and A and V_{ij} represents a second-rank intermolecular coupling tensor, acting between the electronically excited emitter and ground state detector in this instance, which is written as:

$$V_{ij}(k,\mathbf{R}_{DA}) = \frac{\exp(ikR)}{4\pi\varepsilon_0 R^3}\left[(1-ikR)\left(\delta_{ij} - 3\hat{R}_i\hat{R}_j\right) - k^2R^2\left(\delta_{ij} - \hat{R}_i\hat{R}_j\right)\right]. \quad (10.38)$$

Written in this form, the matrix element accommodates both near- and far-field limits as asymptotes $kR_{DA} \ll 1$ and $kR_{DA} \gg 1$, respectively. The remaining higher-order (B-dependent) terms in Eq. (10.36) correspond to different combinations of the interacting nanoemitters and the detector, and relate to the following matrix element contributions:

$$\begin{aligned} M^{DAB} &= \mu_i^{\nu 0}(D)V_{ij}(k,\mathbf{R}_{DA})\alpha_{jk}^{0\alpha}(A,-k;0)V_{kl}(0,\mathbf{R}_{AB})\mu_l^{00}(B)\,, \\ M^{DBA} &= \mu_i^{\nu 0}(D)V_{ij}(k,\mathbf{R}_{DB})\alpha_{(jk)}^{00}(B,-k;k)V_{kl}(k,\mathbf{R}_{AB})\mu_l^{0\alpha}(A)\,, \\ M^{BDA} &= \mu_i^{00}(B)V_{ij}(0,\mathbf{R}_{DB})\alpha_{jk}^{\nu 0}(D,k;0)V_{kl}(k,\mathbf{R}_{DA})\mu_l^{0\alpha}(A), \end{aligned} \quad (10.39)$$

which feature both the index-symmetric molecular polarizability $\alpha_{(jk)}^{00}$ and non-index symmetric forms of the two-photon tensor defined by Eq. (10.12). In principle, all four terms of Eqs. (10.37) and (10.39) contribute to M^A, as each connects the same initial and final system states. Since it is the modulus square of M^A that relates to the observable rate of fluorescence (using Fermi's rule), the result will clearly include cross-terms signifying quantum interference between the various contributions. The lead term for the emission rate is the modulus square of Eq. (10.37), and the interferences between M^{DA} and each of the three higher-order amplitudes (M^{DAB}, M^{DBA} or M^{BDA}) will represent significant corrections. The exact nature of the leading correction term is primarily determined by considering the relative positions of the three components, although selection rules and molecular properties also need to be considered since, for example, the appearance of the static electric dipole $\boldsymbol{\mu}^{00}$ in terms M^{DAB} and M^{BDA} means that B cannot be non – polar if they are to contribute.

In case (b), significant additional effects may arise as result of delocalization of a single initial excitation across the pair, when both nanoemitters are identical. Such circumstances involve the formation of an exciton, and the corresponding quantum state (which follows the initial excitation) is described by a superposition of two localized-excitation states – in either a symmetric $|i^+\rangle$ or an antisymmetric $|i^-\rangle$ combination, *i.e.*:

$$\left|i^{\pm}\right\rangle = 2^{-1/2}|D_0\rangle\left(|A_\alpha\rangle|B_0\rangle \pm |A_0\rangle|B_\alpha\rangle\right) \quad (10.40)$$

where the subscripts label the excited or unexcited state of each participant chromophore. The nanoemitter pair may undergo fluorescent emission from either of the two excitonic states, and the latter corresponds to the following matrix elements;

$$M_{\pm} = 2^{-1/2}\left(M^A \pm M^B\right) \quad (10.41)$$

in which the superscripts designate the effective position of the localized excitation, and the difference in signs is equivalent to introducing a π-phase difference between the two emitters. In situations where molecular coupling is small, the result may be reduced to $\left|M^A\right|^2 + \left|M^B\right|^2$ which corresponds to independent (non-interfering) emitters. Otherwise, the fluorescence signals will relate to symmetric, $|M_+|^2$, or anti-symmetric, $|M_-|^2$, excitonic emission.

Cast in terms of the electric field created from the strongly coupled emitter pair, achieved by excluding $\mu_i^{\nu 0}(D)$ from the relevant matrix elements (*i.e.* either the symmetric or anti-symmetric case), the distribution in optical phase is found from the argument of the electric field – more detail is given later. Figure 10.4 show plots of the fluorescence emitted from a pair of coupled molecules in symmetric and anti-symmetric configurations, with the colors representing the optical phase distribution. For the purposes of the graphs, the transition dipole moments of A and B are perpendicular to the exhibited plane. On comparing the two types of pairwise excitonic emission, it is apparent that a nodal plane (corresponding to no fluorescence signal) appears for antisymmetric situations when the detector is equidistant from both A and B, which is visibly distinct from symmetric emission. In any case, such contour maps reveal striking departures from the known character of single-center emission [85].

10.5.2 Multi-emitter Systems: Generators of Vortex Light

Given a larger number of identical nanoemitters it is possible, by satisfying certain phase and symmetry constraints, to produce fluorescence whose phase distribution twists around an axis of phase singularity; this is the phenomenon known as an 'optical vortex' or 'twisted' beam. Vortex beams, whose existence was first entertained in a series of works [86–89], are characterized by a helical wavefront, based on the azimuthal progression of phase around a singular axis. The production of such beams, which is now experimentally routine, has proven that they convey orbital angular momentum (OAM) – an attribute that is separate from the more familiar spin angular momentum associated with circular polarizations [90]. Ongoing advances have allowed the quantum nature of such beams to be fully elicited [91]. The structure is primarily dependent on the topological charge, l (signifying an OAM of $l\,\hbar$ per photon) an integer that can be either positive or negative – denoting left- or right-handed gyration, respectively, of the light. A beam with a topological charge l has a field distribution in the form of l intertwined helices, each completing a turn of 2π radians about the axis over a span of l wavelengths [92–94]. Whereas the production of vortex light usually involves imparting OAM onto a laser beam with a more common mode structure; [95–102] it has only recently emerged that

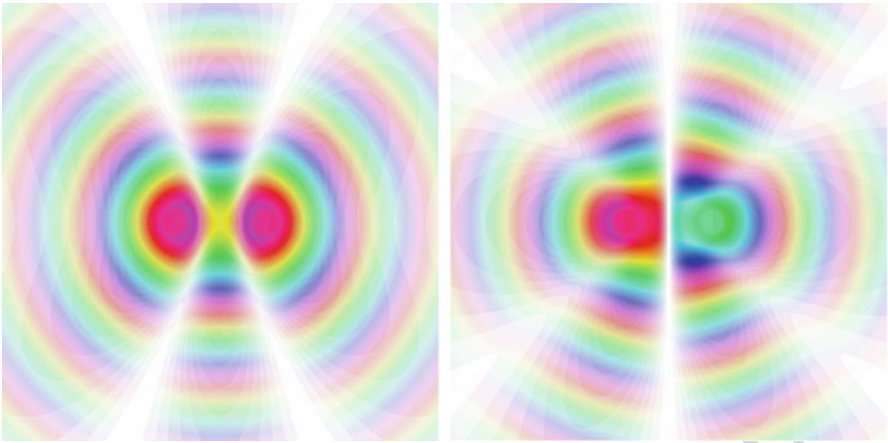

Fig. 10.4 Plots of the fluorescence measured at the detector, with colors representation of the optical phase distribution. Brightness and color hue relate to the modulus and complex argument of the fields emitted by symmetric (*left*) and antisymmetric (*right*) excitons

such light can indeed be directly produced in the fluorescent decay of a set of coupled nanoemitters, as illustrated in Fig. 10.5 [103–105].

For the sought effect to occur, the electromagnetically coupled nanoemitters once again have to sustain an exciton, delocalized across the array. The relative orientations of the molecular dipole moments are crucially important for producing vortex light. It transpires that the array must belong to one of the Schoenflies point groups C_n, C_{nh}, S_n, T, T_h, where n is the number of nanoemitters; the example shown in Fig. 10.5 has C_7 symmetry. Table 10.1 provides the possible integer values of OAM for vortex light emitted from a nanoarray belonging to one of the C_n and C_{nh} point groups [105].

In the decay transitions that accompany the relaxation of the excitonic states – assumed to terminate in a totally symmetric ground electronic state – the symmetry character of the initial exciton maps directly onto the vortex structure of the emitted light. It is therefore necessary to determine the form of the requisite excitons. A block diagonalized form of the array Hamiltonian is required, with the single delocalized excitonic state as a basis. In general, the matrix form of the array Hamiltonian is expressible as follows:

$$H_{rs} = E_u \delta_{rs} + (\boldsymbol{\mu}_r . \mathbf{V}(\mathbf{R}_{rs}) . \boldsymbol{\mu}_s)\left(\delta_{r-1,s(\mathrm{mod}n)} + \delta_{r(\mathrm{mod}n),s-1}\right) \tag{10.42}$$

where each element of the n-square matrix relates to a pair of emitters $\{r, s\}$. Each diagonal element $E_u = \hbar c k_u$ signifies the energy of an isolated nanoemitter in its excited electronic level u. The off – diagonal elements, denoting pairwise interactions, involve the electrodynamic coupling $\mathbf{V}(\mathbf{R}_{rs})$ between neighboring transition dipole moments $\boldsymbol{\mu}_r$ and $\boldsymbol{\mu}_s$ – and all are identical, *i.e.*:

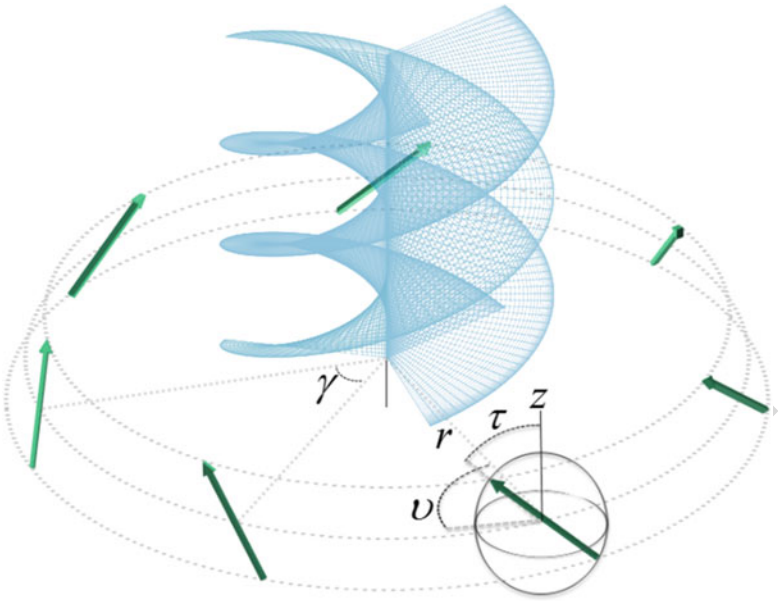

Fig. 10.5 Schematic depiction for a ring of seven molecular nanoemitters, positioned such that their transition moments form a ring whose normal lies in the z-direction. Emission from the lowest energy exciton state releases a photon with topological charge $l = 3$ along the normal axis, with a helicoid evolvement of each wavefront component signifying a surface of constant phase. The angle γ designates the azimuthal position in the plane; τ and υ are angles that specify the local orientation of each emitter. Dotted lines are guides for the eye

Table 10.1 Summary of permitted topological charges, l values, for OAM outputs from nanoarrays with the required symmetry

Number of emitters	Symmetry group	
	C_n, C_{nh}	S_n
3	1	–
4	1	1
5	1,2	–
6	1,2	1
7	1,2,3	–
8	1,2,3	1,2,3
9	1,2,3,4	–
10	1,2,3,4	1,2

$$\mathbf{V}(\mathbf{R}_{rs}) \equiv V_{r,(r+1)\mathrm{mod}n}\left(k_u, \mathbf{R}_{r,(r+1)\mathrm{mod}n}\right). \tag{10.43}$$

Here, $\mathbf{R}_{rs}$ is the vector displacement between the relevant nanoemitters: R is defined by $\mathbf{R}_r - \mathbf{R}_s \equiv \mathbf{R}_{rs} = R\hat{\mathbf{R}}_{rs}$. Under the described symmetry conditions, all the non-zero off – diagonal elements of Eq. (10.43) return the same scalar value, U, given by;

$$
\begin{aligned}
U &= \boldsymbol{\mu}_r.\mathbf{V}(\mathbf{R}_{rs}).\boldsymbol{\mu}_s \\
&\equiv \frac{e^{ik_uR}}{4\pi\varepsilon_0 R^3}\Big[\Big\{1 - ik_uR - (k_uR)^2\Big\}\big(\boldsymbol{\mu}_1^{0u}\cdot\boldsymbol{\mu}_2^{0u}\big) \\
&\quad -\Big\{3 - 3ik_uR - (k_uR)^2\Big\}\big\{\big(\boldsymbol{\mu}_1^{0u}\cdot\hat{\mathbf{R}}_{12}\big)\big(\boldsymbol{\mu}_2^{0u}\cdot\hat{\mathbf{R}}_{12}\big)\big\}\Big].
\end{aligned}
\tag{10.44}
$$

for any specific pair arbitrarily labelled 1 and 2. The eigenfunctions now emerge as normalized superpositions of the basis states:

$$
\big|\psi_p\big\rangle = \frac{1}{\sqrt{n}}\sum_{r=1}^{n}\varepsilon_n^{(r-1)p}\big|\xi^{r;u}\big\rangle\prod_{s\neq r}\big|\xi^{s;0}\big\rangle,\ p\in\{1,\ldots,n\}. \tag{10.45}
$$

Here, $|\xi^{r;u}\rangle$ is a state function corresponding to an emitter r in electronic state u, and $\varepsilon_n = \exp(2\pi i/n)$. In every summand of Eq. (10.45), one molecule is in the electronically excited state u, while the others are in their ground states. The energy eigenvalues associated with the above exciton states are generally expressible in the form;

$$
E_p = E_u + 2U\cos(2pq/n)\ , \tag{10.46}
$$

with the permissible range of values for the index q as indicated in Table 10.2 which also indicates, for the first few point groups C_n, the irreducible representation associated with each excitonic state.

Due to their differences in symmetry, the various exciton eigenstates with representations E_q, A (and also B, if present) will also exhibit differences in energy, manifest as line splittings centered upon the frequency of an isolated emitter. For example in a nanoarray with $n = 3$ emitters, the positioning of exciton levels leads to one non-degenerate state (belonging to the totally symmetric representation A), of energy $E_u - 2U$, and two doubly degenerate (E representation) states of energy $E_u + U$. Furthermore, the sign of the coupling U is readily shown to be positive for all $n \geq 3$, producing splitting patterns as exemplified in Fig. 10.6. Attention now focuses on exciton E states belonging to doubly degenerate irreducible representations. These excitons exist in the form of pairs, one with a left-handed and the other a right-handed progression of phase around the ring. These states exactly correspond with the sought distributions of phase about the symmetry axis, and are separated in energy from the A form – a principle that should enable the selective excitation of one symmetry type. The decay of each doubly degenerate exciton can therefore release a photon with a characteristic long wavelength; in most cases, the exciton pair with the lowest energy will be associated with the highest values of $|q|$ and, as it emerges, the largest topological charge for the emitted vortex.

Finally, to map the optical phase of the fluorescence, an expression for the electric field $\mathbf{E}_p\ (\mathbf{R}_D)$ from each constituent nanoemitter is required, *i.e.*:

Table 10.2 List of the irreducible representations (irreps) of the C_n exciton states for $n = 3$–7

n	p	1	2	3	4	5	6	7
3	q	1	-1	0				
	Irrep	E_1	E_1	A				
4	q	1	2	-1	0			
	Irrep	E_1	B	E_1	A			
5	q	1	2	-2	-1	0		
	Irrep	E_1	E_2	E_2	E_1	A		
6	q	1	2	3	-2	-1	0	
	Irrep	E_1	E_2	B	E_2	E_1	A	
7	q	1	2	3	-3	-2	-1	0
	Irrep	E_1	E_2	E_3	E_3	E_2	E_1	A

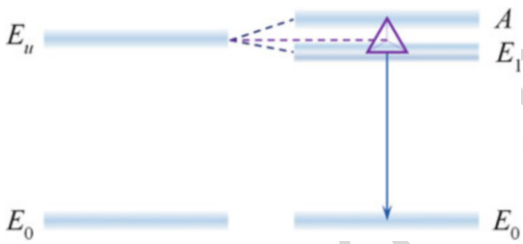

Fig. 10.6 Excitonic irreducible representations and Davydov energy level splitting of for an array of C_3 point group symmetry. The splitting between A and E_1 equal to $3U$. The three-emitter case, as indicated by the relaxation arrow, will have a preferential $|q| = 1$ emission

$$\mathbf{E}_p(\mathbf{R}_D) = \sum_r^n \frac{e^{ikR_{Dr}}\varepsilon_n^{(r-1)p}}{4\pi\varepsilon_0 R_{Dr}^3}\left\{\left[\left(\hat{\mathbf{R}}_{Dr} \times \boldsymbol{\mu}_r^{0u}\right) \times \hat{\mathbf{R}}_{Dr}\right]k^2R_{Dr}^2 + \left[3\hat{\mathbf{R}}_{Dr}\left(\hat{\mathbf{R}}_{Dr} \cdot \boldsymbol{\mu}_r^{0u}\right) - \boldsymbol{\mu}_r^{0u}\right](1 - ikR_{Dr})\right\}, \tag{10.47}$$

where $\mathbf{R}_D$ signifies the displacement, relative to the ring center, of a point of measurement or detection. Notably, each term in Eq. (10.47) carries the phase factor $\varepsilon_n^{(r-1)p}$, from the corresponding emitter component in Eq. (10.45), thus delivering the sought progression in phase around the ring. At any point in space, the most appropriate measure of the phase for the emitted radiation is the function defined by:

$$\theta_i(\mathbf{R}) = \arg\left\{\mathbf{E}_{p;\,i}(\mathbf{R}_D)\right\}\ , \tag{10.48}$$

the principle argument of the complex electric field vector. Typical maps of the electromagnetic phase distributions, shown in Fig. 10.7, exhibit the variation of the phase in planes parallel to the source array, for several combinations of molecular number and exciton symmetry. The panes in this figure show rings with three and six chromophore components, the latter having two topological charges. The phase properties of the electromagnetic fields emitted by the arrays in each case map

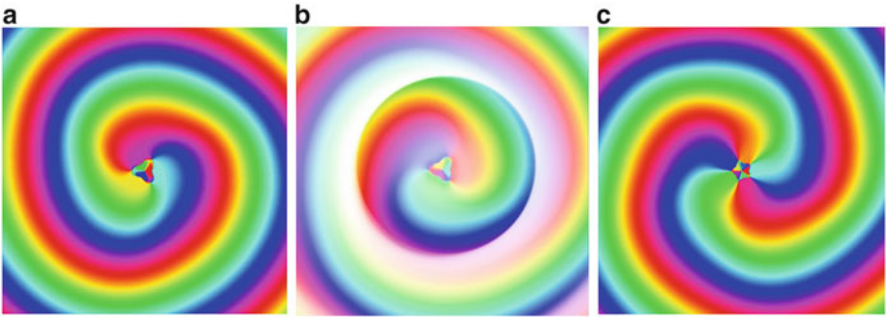

Fig. 10.7 Cross-sectional simulations of the scalar optical field in the array plane supporting optical vortex emission: (**a**) three chromophores, emission with topological charge $l = 1$; (**b**) also three chromophores $l = -1$, here also showing (by color intensity) the field magnitude; (**c**) five chromophores supporting $l = -2$ emission

exactly to the azimuthal phase dependence of a vortex mode. Such arrays thus represents systems whose fluorescence can naturally generate optical vorticity, without requiring any of the transformation optics that might otherwise need to be deployed [106–109].

10.6 Discussion

This review has endeavored to show that, by developing a fully photon-based representation of conventional molecular fluorescence, a variety of other closely related phenomena can readily be identified in the same quantum field framework of theory. The most familiar variant, multiphoton fluorescence, is sufficiently well established that it has already found advanced applications in optical diagnostics in biology and medicine. Laser-controlled and multi-emitter fluorescence represent more recent arrivals on the scene, and in these cases experimental work has not yet quite caught up with the developments in theory. Each topic holds promise for a range of new kinds of application. For example the capacity to modify fluorescence with an auxiliary beam opens new ground for excited state lifetime manipulation, all-optical switching devices – and potentially even an all-optical transistor [54]. Equally, with advances in nanofabrication paving the way for the batch production of tailored nanoemitter arrays, the potential of materials that can directly generate optical vortex light is also becoming enticing, particularly in view of the associated capacity to convey significantly more information per photon [110, 111]. In other areas, too, the science is still advancing apace. For example, building on the well-known theory of circularly polarized luminescence [112], there is now fresh interest in establishing signatures of chirality in the fluorescence produced by chiral molecules [113]. It will be fascinating to see where the next advance will arise.

References

1. Wilcox CH (1966) Perturbation theory and its applications in quantum mechanics. Wiley Chapman and Hall, New York/London
2. Grynberg G, Aspect A, Fabre C (2010) Introduction to quantum optics: from the semi-classical approach to quantized light. Cambridge University Press, Cambridge
3. Andrews DL, Bradshaw DS, Coles MM (2011) Perturbation theory and the two-level approximation: a corollary and critique. Chem Phys Lett 503:153–156
4. Kmetic MA, Meath WJ (1985) Permanent dipole moments and multi-photon resonances. Phys Lett A 108:340–343
5. Kondo AE, Meath WJ, Nilar SH, Thakkar AJ (1994) Pump-probe studies of the effects of permanent dipoles in one- and two-colour molecular excitations. Chem Phys 186:375–394
6. Jagatap BN, Meath WJ (1996) On the competition between permanent dipole and virtual state two-photon excitation mechanisms, and two-photon optical excitation pathways, in molecular excitation. Chem Phys Lett 258:293–300
7. Spano FC, Mukamel S (1989) Nonlinear susceptibilities of molecular aggregates: enhancement of X(3) by size. Phys Rev A 40:5783–5801
8. Leegwater JA, Mukamel S (1992) Exciton-scattering mechanism for enhanced nonlinear response of molecular nanostructures. Phys Rev A 46:452–464
9. Mukamel S (1995) Principles of nonlinear optical spectroscopy. Oxford University Press, New York
10. Venkatramani R, Mukamel S (2005) Dephasing-induced vibronic resonances in difference frequency generation spectroscopy. J Phys Chem B 109:8132–8143
11. Zrenner A, Beham E, Stufler S, Findeis F, Bichler M, Abstreiter G (2002) Coherent properties of a two-level system based on a quantum-dot photodiode. Nature 418:612
12. Klimov VI (2003) Nanocrystal quantum dots. Los Alamos Sci 28:214
13. Kirkpatrick SM, Naik RR, Stone MO (2001) Nonlinear saturation and determination of the two-photon absorption cross section of green fluorescent protein. J Phys Chem B 105:2867–2873
14. Stufler S, Ester P, Zrenner A, Bichler M (2005) Quantum optical properties of a single $In_xGa_{1-X}As$ – GaAs quantum dot two-level system. Phys Rev B 72:121301
15. Drobizhev M, Marakov NS, Hughes T, Rebane AJ (2007) Resonance enhancement of two-photon absorption in fluorescent proteins. J Phys Chem B 111:14051–14054
16. Asselberghs I, Flors C, Ferrighi L, Botek E, Champagne B, Mizuno H, Ando R, Miyawaki A, Hofkens J, Van der Auweraer M, Clays K (2008) Second-harmonic generation in Gfp-like proteins. J Am Chem Soc 130:15713–15719
17. Drobizhev M, Tillo S, Makarov NS, Hughes TE, Rebane AJ (2009) Color hues in red fluorescent proteins are due to internal quadratic stark effect. J Phys Chem B 113:12860–12864
18. Beuerman E, Makarov NS, Drobizhev M, Rebane AJ (2010) Justification of two-level approximation for description of two-photon absorption in oxazine dyes. Proc SPIE 7599:75990X
19. Andrews DL, Dávila Romero LC, Meath WJ (1999) An algorithm for the nonlinear optical susceptibilities of dipolar molecules, and an application to third harmonic generation. J Phys B At Mol Opt Phys 32:1–17
20. Juzeliūnas G, Dávila Romero LC, Andrews DL (2003) Eliminating ground-state dipole moments in quantum optics via canonical transformation. Phys Rev A 68:043811
21. Lakowicz JR (1999) Principles of fluorescence spectroscopy, 2nd edn. Kluwer, New York
22. Valeur B, Berberan-Santos MN (2013) Molecular fluorescence: principles and applications, 2nd edn. Wiley-VCH, Weinheim
23. Inoué S, Shimomura O, Goda M, Shribak M, Tran PT (2002) Fluorescence polarization of green fluorescence protein. Proc Natl Acad Sci U S A 99:4272–4277

24. Brasselet S, Le Floc'h V, Treussart F, Roch J-F, Zyss J (2004) In situ diagnostics of the crystalline nature of single organic nanocrystals by nonlinear microscopy. Phys Rev Lett 92:207401
25. Gasecka A, Dieu L-Q, Brühwiler D, Brasselet S (2010) Probing molecular order in zeolite L inclusion compounds using two-photon fluorescence polarimetric microscopy. J Phys Chem B 114:4192–4198
26. Corry B, Jayatilaka D, Martinac B, Rigby P (2006) Determination of the orientational distribution and orientation factor for transfer between membrane-bound fluorophores using a confocal microscope. Biophys J 91:1032–1045
27. Gasecka A, Han T-J, Favard C, Cho BR, Brasselet S (2009) Quantitative imaging of molecular order in lipid membranes using two-photon fluorescence polarimetry. Biophys J 97:2854–2862
28. Empedocles SA, Neuhauser R, Bawendi MG (1999) Three-dimensional orientation measurements of symmetric single chromophores using polarization microscopy. Nature 399:126–130
29. Weiss S (2000) Measuring conformational dynamics of biomolecules by single molecule fluorescence spectroscopy. Nat Struct Biol 7:724–729
30. Weston KD, Goldner LS (2001) Orientation imaging and reorientation dynamics of single dye molecules. J Phys Chem B 105:3453–3462
31. Vacha M, Kotani M (2003) Three-dimensional orientation of single molecules observed by far- and near-field fluorescence microscopy. J Chem Phys 118:5279–5282
32. Festy F, Ameer-Beg SM, Ng T, Suhling K (2007) Imaging proteins in vivo using fluorescence lifetime microscopy. Mol Biosyst 3:381–391
33. Levitt JA, Matthews DR, Ameer-Beg SM, Suhling K (2009) Fluorescence lifetime and polarization-resolved imaging in cell biology. Curr Opin Biotechnol 20:28–36
34. Gradinaru CC, Marushchak DO, Samim M, Krull UJ (2010) Fluorescence anisotropy: from single molecules to live cells. Analyst 135:452
35. Loudon R (2000) The quantum theory of light, 3rd edn. Oxford University Press, Oxford
36. Meath WJ, Power EA (1984) On the importance of permanent moments in multiphoton absorption using perturbation-theory. J Phys B At Mol Opt Phys 17:763–781
37. Andrews DL, Thirunamachandran T (1977) Polarization effects in nonlinear scattering. Opt Commun 22:312–314
38. Andrews DL, Blake NP (1989) Three-dimensional rotational averages in radiation molecule interactions: an irreducible Cartesian tensor formulation. J Phys A Math Gen 22:49–60
39. Friese DH, Beerepoot MTP, Ruud K (2014) Rotational averaging of multiphoton absorption cross sections. J Chem Phys 141:204103
40. McClain WM (1971) Excited state symmetry assignment through polarized two-photon absorption studies of fluids. J Chem Phys 55:2789–2796
41. Monson PR, McClain WM (1972) Complete polarization study of the two-photon absorption of liquid 1-chloronaphthalene. J Chem Phys 56:4817–4825
42. Andrews DL, Ghoul WA (1981) Eighth rank isotropic tensors and rotational averages. J Phys A Math Gen 14:1281–1290
43. Leeder JM, Andrews DL (2011) A molecular theory for two-photon and three-photon fluorescence polarization. J Chem Phys 134:094503
44. Lakowicz JR, Gryczynski I, Malak H, Schrader M, Engelhardt P, Kano H, Hell SW (1997) Time-resolved fluorescence spectroscopy and imaging of DNA labeled with Dapi and Hoechst 33342 using three-photon excitation. Biophys J 72:567–578
45. Kastrup L, Blom H, Eggeling C, Hell SW (2005) Fluorescence fluctuation spectroscopy in subdiffraction focal volumes. Phys Rev Lett 94:178104
46. Hell SW (2007) Far-field optical nanoscopy. Science 316:1153–1158
47. Willig KI, Harke B, Medda R, Hell SW (2007) Sted microscopy with continuous wave beams. Nat Methods 4:915–918

48. Zhou LC, Liu JY, Zhao GJ, Shi Y, Peng XJ, Han KL (2007) The ultrafast dynamics of near-infrared heptamethine cyanine dye in alcoholic and aprotic solvents. Chem Phys 333:179–185
49. Armoogum DA, Marsh RJ, Nicolaou N, Mongin O, Blanchard-Desce M, Bain AJ (2008) Stimulated emission depletion and fluorescence correlation spectroscopy of a branched quadrupolar chromophore. Proc SPIE 7030:70300S
50. Harke B, Keller J, Ullal CK, Westphal V, Schoenle A, Hell SW (2008) Resolution scaling in STED microscopy. Opt Express 16:4154
51. Hell SW (2009) Microscopy and its focal switch. Nat Methods 6:24–32
52. Andrews DL, Bradshaw DS, Jenkins RD, Rodríguez J (2009) Dendrimer light-harvesting: intramolecular electrodynamics and mechanisms. Dalton Trans:10006–10014 AU2
53. Bradshaw DS, Andrews DL (2010) All-optical control of molecular fluorescence. Phys Rev A 81:013424
54. Andrews DL, Bradshaw DS (2010) Optical transistor action by nonlinear coupling of stimulated emission and coherent scattering. Proc SPIE 7797:77970L
55. Leeder JM, Bradshaw DS, Andrews DL (2011) Laser-controlled fluorescence in two-level systems. J Phys Chem B 115:5227–5233
56. Lakowicz JR (2005) Radiative decay engineering 5: metal-enhanced fluorescence and plasmon emission. Anal Biochem 337:171–194
57. Anger P, Bharadwaj P, Novotny L (2006) Enhancement and quenching of single-molecule fluorescence. Phys Rev Lett 96:113002
58. Tam F, Goodrich GP, Johnson BR, Halas NJ (2007) Plasmonic enhancement of molecular fluorescence. Nano Lett 7:496–501
59. Giannini V, Sánchez-Gil JA (2008) Excitation and emission enhancement of single molecule fluorescence through multiple surface-Plasmon resonances on metal trimer nanoantennas. Opt Lett 33:899–901
60. Fort E, Grésillon S (2008) Surface enhanced fluorescence. J Phys D Appl Phys 41:013001
61. Lin C-Y, Chiu K-C, Chang C-Y, Chang S-H, Guo T-F, Chen S-J (2010) Surface plasmon-enhanced and quenched two-photon excited fluorescence. Opt Express 18:12807–12817
62. Lu G, Zhang T, Li W, Hou L, Liu J, Gong Q (2011) Single-molecule spontaneous emission in the vicinity of an individual gold nanorod. J Phys Chem C 115:15822–15828
63. Derom S, Berthelot A, Pillonnet A, Benamara O, Jurdyc AM, Girard C, Colas des Francs G (2013) Metal enhanced fluorescence in rare earth doped plasmonic core–shell nanoparticles. Nanotechnology 24:495704
64. Khatua S, Paulo PMR, Yuan H, Gupta A, Zijlstra P, Orrit M (2014) Resonant plasmonic enhancement of single-molecule fluorescence by individual gold nanorods. ACS Nano 8:4440–4449
65. Lu D, Kan JJ, Fullerton EE, Liu Z (2014) Enhancing spontaneous emission rates of molecules using nanopatterned multilayer hyperbolic metamaterials. Nat Nanotechnol 9:48–53
66. Allcock P, Jenkins RD, Andrews DL (2000) Laser-assisted resonance-energy transfer. Phys Rev A 61:023812
67. Andrews DL (2007) Optically switched energy transfer: twin-beam off-resonance control. Phys Rev Lett 99:023812
68. Bradshaw DS, Andrews DL (2008) Optically controlled resonance energy transfer: mechanism and configuration for all-optical switching. J Chem Phys 128:144506
69. Craig DP, Thirunamachandran T (1998) Molecular quantum electrodynamics: an introduction to radiation-molecule interactions. Dover Publications, Mineola
70. Andrews DL, Allcock P (2002) Optical harmonics in molecular systems. Wiley-VCH, Weinheim
71. Kleinman DA, Dielectric N (1962) Polarization in optical media. Phys Rev 126:1977–1979
72. Salam A (2012) Mediation of resonance energy transfer by a third molecule. J Chem Phys 136:014509

73. Andrews DL, Ford JS (2013) Resonance energy transfer: influence of neighboring matter absorbing in the wavelength region of the acceptor. J Chem Phys 139:014107
74. Coles MM, Leeder JM, Andrews DL (2014) Static and dynamic modifications to photon absorption: the effects of surrounding chromophores. Chem Phys Lett 595–596:151–155
75. Leeder JM, Andrews DL (2014) Enhancing optical up-conversion through electrodynamic coupling with ancillary chromophores. J Phys Chem C 118:23535–23544
76. Kühn S, Håkanson U, Rogobete L, Sandoghdar V (2006) Enhancement of single-molecule fluorescence using a gold nanoparticle as an optical nanoantenna. Phys Rev Lett 97:017402
77. Ringler M, Schwemer A, Wunderlich M, Nichtl A, Kürzinger K, Klar TA, Feldmann J (2008) Shaping emission spectra of fluorescent molecules with single plasmonic nanoresonators. Phys Rev Lett 100:203002
78. Bakker RM, Drachev VP, Liu Z, Yuan H-K, Pedersen RH, Boltasseva A, Chen J, Irudayaraj J, Kildishev AV, Shalaev VM (2008) Nanoantenna array-induced fluorescence enhancement and reduced lifetimes. New J Phys 10:125022
79. Vecchi G, Giannini V, Gómez Rivas J (2009) Shaping the fluorescent emission by lattice resonances in plasmonic crystals of nanoantennas. Phys Rev Lett 102:146807
80. Ward DR, Hüser F, Pauly F, Cuevas JC, Natelson D (2010) Optical Rectification and Field Enhancement in a Plasmonic Nanogap. Nat Nanotechnol 5:732–736
81. Novotny L, van Hulst N (2011) Antennas for light. Nat Photonics 5:83–90
82. Agio M (2012) Optical antennas as nanoscale resonators. Nanoscale 4:692–706
83. Lee KG, Eghlidi H, Chen XW, Renn A, Götzinger S, Sandoghdar V (2012) Spontaneous emission enhancement of a single molecule by a double-sphere nanoantenna across an interface. Opt Express 20:23331–23338
84. Rice EM, Andrews DL (2012) Optical emission of a molecular nanoantenna pair. J Chem Phys 136:244503
85. Rice EM, Bradshaw DS, Saadi K, Andrews DL (2012) Identifying the development in phase and amplitude of dipole and multipole radiation. Eur J Phys 33:345–358
86. Nye J, Berry M (1974) Dislocations in wave trains. Proc Royal Soc A Math Phys Eng Sci 336:165–190
87. Coullet P, Gil L, Rocca F (1989) Optical vortices. Opt Commun 73:403–408
88. Saleh BEA, Teich MC (1991) Fundamentals of photonics. Wiley, New York
89. Allen L, Beijersbergen MW, Spreeuw RJC, Woerdman JP (1992) Orbital angular momentum of light and the transformation of Laguerre-Gaussian laser modes. Phys Rev A 45:8185–8189
90. Andrews DL, Babiker M (2013) The angular momentum of light. Cambridge University Press, Cambridge
91. Dávila Romero LC, Andrews DL, Babiker M (2002) A quantum electrodynamics framework for the nonlinear optics of twisted beams. J Opt B Quantum Semiclassical Opt 4:S66
92. Padgett MJ, Courtial J (1999) Poincaré-sphere equivalent for light beams containing orbital angular momentum. Opt Lett 24:430–432
93. Allen L (2002) Introduction to the atoms and angular momentum of light special issue. J Opt B Quantum Semiclassical Opt 4:S1–S6
94. Milione G, Sztul HI, Nolan DA, Alfano RR (2011) Higher-order Poincaré sphere, Stokes parameters, and the angular momentum of light. Phys Rev Lett 107:053601
95. Heckenberg NR, McDuff R, Smith CP, White AG (1992) Generation of optical-phase singularities by computer-generated holograms. Opt Lett 17:221–223
96. Bazhenov VY, Soskin M, Vasnetsov M (1992) Screw dislocations in light wavefronts. J Mod Opt 39:985–990
97. Beijersbergen MW, Allen L, Vanderveen HELO, Woerdman JP (1993) Astigmatic laser mode converters and transfer of orbital angular-momentum. Opt Commun 96:123–132
98. Beijersbergen MW, Coerwinkel RPC, Kristensen M, Woerdman JP (1994) Helical-wavefront laser-beams produced with a spiral phaseplate. Opt Commun 112:321–327
99. Marrucci L, Manzo C, Paparo D (2006) Optical spin-to-orbital angular momentum conversion in inhomogeneous anisotropic media. Phys Rev Lett 96:163905

100. Mirhosseini M, Magana-Loaiza OS, Chen C, Rodenburg B, Malik M, Boyd RW (2013) Rapid generation of light beams carrying orbital angular momentum. Opt Express 21:30196–30203
101. Sun J, Zeng J, Litchinitser NM (2013) Twisting light with hyperbolic metamaterials. Opt Express 21:14975–14981
102. Ostrovsky AS, Rickenstorff-Parrao C, Arrizón V (2013) Generation of the "perfect" optical vortex using a liquid-crystal spatial light modulator. Opt Lett 38:534–536
103. Coles MM, Williams MD, Andrews DL (2013) Second harmonic generation in isotropic media: six-wave mixing of optical vortices. Opt Express 21:12783–12789
104. Williams MD, Coles MM, Saadi K, Bradshaw DS, Andrews DL (2013) Optical vortex generation from molecular chromophore arrays. Phys Rev Lett 111:153603
105. Williams MD, Coles MM, Bradshaw DS, Andrews DL (2014) Direct generation of optical vortices. Phys Rev A 89:033837
106. García-García J, Rickenstorff-Parrao C, Ramos-García R, Arrizón V, Ostrovsky AS (2014) Simple technique for generating the perfect optical vortex. Opt Lett 39:5305–5308
107. Karimi E, Schulz SA, De Leon I, Qassim H, Upham J, Boyd RW (2014) Generating optical orbital angular momentum at visible wavelengths using a plasmonic metasurface. Light Sci Appl 3:e167
108. Andrews DL, Williams MD, Bradshaw DS, Lui R, Phillips DB, Franke-Arnold S, Padgett MJ (2014) Nanoarrays for the generation of complex optical wave-forms. Proc SPIE 9160:91601L
109. Liu R, Phillips DB, Li F, Williams MD, Andrews DL, Padgett MJ (2015) Discrete emitters as a source of orbital angular momentum. J Opt 17:045608
110. Franke-Arnold S, Jeffers J (2008) Orbital angular momentum in quantum communication and information. In: Andrews DL (ed) Structured light and its applications: an introduction to phase-structured beams and nanoscale optical forces. Academic, Amsterdam/Boston, pp 271–291
111. Mirhosseini M, Magaña-Loaiza OS, O'Sullivan MN, Rodenburg B, Malik M, Lavery MPJ, Padgett MJ, Gauthier DJ, Boyd RW (2015) High-dimensional quantum cryptography with twisted light. New J Phys 17:033033
112. Riehl JP, Richardson FS (1993) Circularly polarized luminescence. Methods Enzymol 226:539–553
113. Bradshaw DS, Leeder JM, Coles MM, Andrews DL (2015) Signatures of material and optical chirality: origins and measures. Chem Phys Lett 626:106–110

Author Queries

Chapter No.: 10 352800_1_En

Query Refs.	Details Required	Author's response
AU1	Please confirm the inserted citation for Fig. 10.3.	
AU2	Please provide volume number for Ref. [52].	